Materials Today Bio 32 (2025) 101764

Contents lists available at ScienceDirect

Materials Today Bio

journal homepage: www.journals.elsevier.com/materials-today-bio

Fabrication of GDNF-Gel/HA-Mg nerve conduit and its role in repairing peripheral nerve defects

Yuanqing Cai [a,1], Yi Chen [b,1], Hongyan Li [a,1], Yanyu Wang [c,1], Guangyang Zhang [d], Jialin Liang [d], Leifeng Lv [d], Ying Huang [a], Wenming Zhang [a], Xiaoqian Dang [d,*], Xinyu Fang [a,**], Yong Wang [b,***]

[a] Department of Orthopaedic Surgery, The First Affiliated Hospital, Fujian Medical University, Fuzhou, 350005, China
[b] College of Materials Science & Engineering, National Engineering Research Center for Magnesium Alloys, Chongqing University, Chongqing, 400045, China
[c] Fujian University of Traditional Chinese Medicine, Fuzhou, 350003, China
[d] Department of Orthopaedics, The Second Affiliated Hospital of Xi'an Jiaotong University, Xi'an, 710006, China

ARTICLE INFO

Keywords:
Magnesium
Conduit
Corrosion resistance
Schwann cells
Peripheral nerve regeneration

ABSTRACT

Background: Magnesium (Mg) and its alloys are receiving increasing attention in peripheral nerve regeneration, but they were limited due to the low corrosion resistance and rapid degradation. In this study, GDNF-Gel/HA-Mg was prepared and its value in peripheral nerve defects repairment was explored both *in vitro* and *in vivo*.

Methods: A hydroxyapatite (HA) coating was first applied to the pure Mg surface, followed by the formation of gelatin methacrylate (GelMA) loaded with glial cell-derived neurotrophic factor (GDNF) on the HA-coated Mg surface. GDNF-Gel/HA-Mg corrosion resistance was explored. The effect of GDNF-Gel/HA-Mg conduit on Schwann cell proliferation and migration abilities were investigated. And sciatic nerve defects models were established to explored the role of GDNF-Gel/HA-Mg conduit in peripheral nerve defects repairment.

Findings: The electrochemical, immersion, and hydrogen evolution experiments indicated that the corrosion resistance in phosphate buffer saline (PBS) of pure Mg was significantly improved by the GDNF-Gel/HA coating. Cell cycle, Cell Count Kit-8 (CCK-8), and clone formation assays indicated that GDNF-Gel/HA-Mg promoted the proliferation of Schwann cells. Scratch and Transwell assay results demonstrated that GDNF-Gel/HA-Mg promoted Schwann cell migration ability dose-dependently. GDNF-Gel/HA-Mg was found to enhance the secretion of nerve growth factor (NGF) and the expression of $p75^{NTR}$. Flow cytometry results showed that GDNF-Gel/HA-Mg could reduce H_2O_2-induced oxidative stress and Schwann cell apoptosis. GDNF-Gel/HA-Mg inhibited M1 macrophage polarization while facilitated M2 macrophage polarization in a concentration-dependent manner. The *in vivo* studies demonstrated that GDNF-Gel/HA-Mg conduit could significantly promote the regeneration and myelination of sciatic nerve, as well as the recovery of denervated gastrocnemius atrophy.

Interpretation: The GDNF-Gel/HA-Mg conduit prepared in this study exhibited good hydrophilicity and corrosion resistance and greatly enhanced the proliferation, migration, and invasion abilities of Schwann cells, as well as peripheral nerve regeneration.

This article is part of a special issue entitled: Multiscale Composites published in Materials Today Bio.

* Corresponding author. Department of Orthopaedics, The Second Affiliated Hospital of Xi'an Jiaotong University, No.157, Xiwu Road, Xi'an, 710004, Shaanxi, China.

** Corresponding author. Department of Orthopaedic Surgery, the First Affiliated Hospital, Fujian Medical University, No.20, Chazhong Road, Fuzhou, 350005, Fujian, China.

*** Corresponding author. College of Materials Science & Engineering, National Engineering Research Center for Magnesium Alloys, Chongqing University, No. 174 Shazheng Street, Shapingba District, Chongqing, 400044, China.

E-mail addresses: dangxiaoqian@xjtu.edu.cn (X. Dang), fangxinyu0417@fjmu.edu.cn (X. Fang), yongwangmse@cqu.edu.cn (Y. Wang).

[1] These authors contributed equally to this work.

https://doi.org/10.1016/j.mtbio.2025.101764
Received 4 March 2025; Received in revised form 5 April 2025; Accepted 11 April 2025
Available online 12 April 2025

1. Research in context

1.1. Evidence before this study

Magnesium (Mg) and its alloys have gained increasing attention in peripheral nerve regeneration due to their biodegradability and favorable mechanical properties. However, their clinical application has been limited by rapid degradation and low corrosion resistance, leading to compromised structural integrity and potential cytotoxicity. Various surface modifications, such as hydroxyapatite (HA) coating and polymer-based functionalization, have been explored to improve Mg corrosion resistance and biocompatibility. Additionally, glial cell-derived neurotrophic factor (GDNF) has been recognized for its critical role in supporting Schwann cell function, promoting nerve regeneration, and enhancing neuroprotection. While previous studies have investigated Mg-based scaffolds and neurotrophic factor delivery separately, there remains a lack of research on integrating HA-modified Mg with GDNF to optimize peripheral nerve regeneration.

1.2. Added value of this study

This study successfully developed a novel GDNF-Gel/HA-Mg conduit that combines the benefits of HA coating for corrosion resistance and controlled GDNF release for enhanced nerve regeneration. The findings demonstrate that this biomaterial significantly improves stability of Mg in physiological environments, promotes Schwann cell proliferation and migration, reduces oxidative stress-induced apoptosis, and modulates macrophage polarization toward a pro-regenerative phenotype. Furthermore, *in vivo* experiments confirmed that the GDNF-Gel/HA-Mg conduit enhances sciatic nerve regeneration, myelination, and functional recovery. This study represents a significant advancement in biomaterial-based strategies for peripheral nerve repair by providing a bioactive, biodegradable, and neurotrophic-enhanced Mg scaffold.

1.3. Implications of all the available evidence

The findings of this study, combined with existing evidence, underscore the potential of GDNF-Gel/HA-Mg as a promising strategy for peripheral nerve regeneration. The improved corrosion resistance and bioactivity of the conduit address critical limitations of traditional Mg-based materials, while the sustained release of GDNF enhances Schwann cell function and nerve repair. The ability of GDNF-Gel/HA-Mg to modulate macrophage polarization further supports its role in creating a regenerative microenvironment. These results suggest that the GDNF-Gel/HA-Mg conduit could serve as an effective therapeutic option for peripheral nerve defects, bridging the gap between material science and clinical application. Future research should focus on long-term *in vivo* performance and translational studies to validate its potential for clinical use.

2. Introduction

Peripheral nerve injury (PNI) occurs when external forces, such as open limb injuries, disrupt the nerve trunks and branches of peripheral nerves [1] This disruption leads to impaired nerve conduction, axonal interruption, or complete nerve discontinuity, resulting in sensory, motor, and autonomic dysfunction in the affected limbs [2,3]. Provided that the defects are short-distance and free from infection or excessive tension, end-to-end anastomosis can be performed to repair them [4]. For long defects, the most commonly employed treatment strategy is autograft or allograft nerve transplantation [5,6]. Nonetheless, autograft nerve transplantation is limited by the availability of nerve sources, pain at the donor site, and the risk of infection [5]. Furthermore, autografts are not suitable for longer or larger nerve defects. On the other hand, therapeutic risks such as immune rejection and transmission of infectious diseases are big concerns of allograft or xenograft nerve transplantation [5].

Nerve conduits offer a stable mechanical support for regenerating peripheral nerve defects allowing the growth of nerve fibers towards the distal end [7]. Thus, they can be used as alternatives to autografts or allografts for bridging repairs of peripheral nerve defect ends, especially for the longer or larger defects [8,9]. Nerve conduits are primarily made of natural or synthetic materials. Common natural materials include vein tubes, artery tubes, amniotic membrane tubes, etc [10–12]. These materials facilitate the adhesion and growth of Schwann cells due to their highly consistent basement membrane with the cells. However, nerve conduits made from natural materials have limitations such as susceptibility to deformation, limited availability of materials, and infiltration of fibrous tissue granulation [13,14]. Synthetic nerve conduits are biologically inert, which can lead to complications such as fibrosis of regenerating nerve fibers and chronic nerve compression [12,15]. Hence, it is imperative to develop novel biodegradable materials that can be used in nerve conduits, so as to improve the therapeutic outcomes for PNI.

Magnesium (Mg), which ranks as the fourth most abundant mineral ion in the human body, plays a vital role in physiological processes [16]. It is involved in cellular energy metabolism, synthesis of nucleic acids, proteins, and cytokines, regulation of transporters and ion channels, and integrity of cell membranes [17,18]. It has been demonstrated that Mg acts as a neuroprotective agent [19,20], that is, Mg modulates cellular functions, antagonizes N-methyl-D-aspartate (NMDA) receptors, counteracts calcium overload, and reduces secondary damage [19]. In the application of repairing PNI, Mg offers several benefits [20]. Firstly, Mg shows excellent biocompatibility, without damage to the nerve tissue [19,21]. Secondly, Mg is biodegradable, which is very important for long-term nerve repair due to the disappearance of chronic nerve compression caused by a permanent conduit [19]. Thirdly, Mg possesses favorable mechanical properties, providing adequate mechanical support for the damaged nerves, especially at the early stages of repair. Finally, Mg is conductive, enabling the transmission of nerve signals over long distances, facilitating electrical stimulation for the growth of distal nerves, and promoting nerve regeneration and functional recovery [19]. However, the rapid corrosion of magnesium creates a locally alkaline microenvironment, which is not conductive to nerve tissue regeneration [22]. Excessive corrosion rate might also compromise the supportive strength of Mg-based nerve conduits [19]. Moreover, in the process of peripheral nerve regeneration, a variety of neural trophic factors are essential for promoting axonal regrowth. Unfortunately, Mg-based nerve conduits, being metallic constructs, lack the capacity to provide essential nutritional support for nerve regeneration. Additionally, their inherently limited permeability may compromise the effective diffusion of Schwann cell-derived neurotrophic factors to the defect ends.

To further advance the application of Mg-based nerve conduits in peripheral nerve defect repair, it is imperative to enhance their corrosion resistance, regulate their degradation rate, and minimize hydrogen production during degradation. These modifications are crucial for ensuring prolonged mechanical support and precise guidance throughout the nerve regeneration process. Moreover, integrating neurotrophic factors and other bioactive molecules into magnesium-based conduits is essential for augmenting their biological activity. The controlled and sustained release of neurotrophic factors can further facilitate nerve regeneration by creating a bioactive microenvironment conducive to repair. Building upon this concept, our study employed hydroxyapatite (HA) coating modification to develop HA-Mg and incorporated glial cell-derived neurotrophic factor (GDNF) into the Mg-based conduit. By strategically combining enhanced corrosion resistance with improved bioactivity, we prepared a novel nerve conduit—GDNF-Gel/HA-Mg. Through comprehensive *in vitro* and *in vivo* investigations, we systematically evaluated its therapeutic potential and elucidated the underlying mechanisms contributing to peripheral nerve defect repair (Fig. 1).

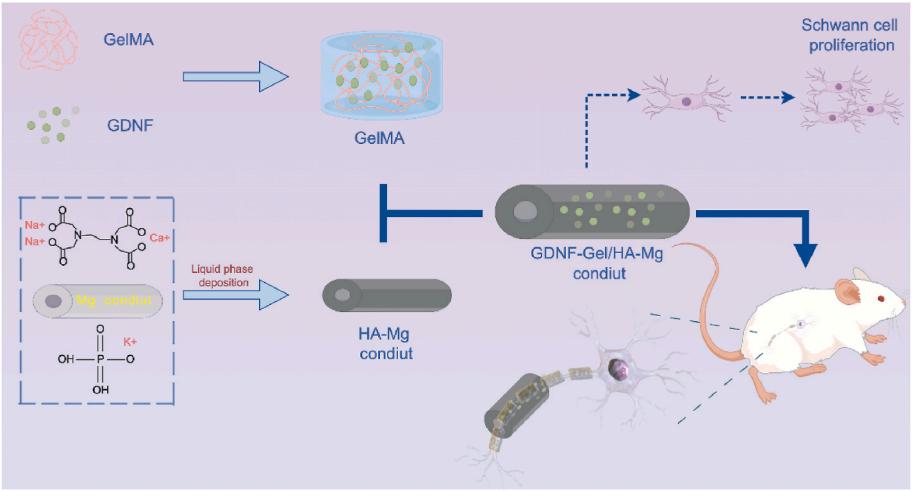

Fig. 1. Graphic abstract: the preparation of GDNF-Gel/HA-Mg conduit and its potential role in peripheral nerve defect repair. Mg: magnesium; HA: hydroxylapatite; GDNF: glial cell line-derived neurotrophic factor; GelMA: Gelatin methacryloyl.

3. Methods

3.1. Preparation of GDNF-Gel/HA-Mg material

Mg conduits and flakes (conduits: 12 mm in length, with an inner diameter of 2.0 mm and a tube wall thickness of 0.5 mm, flakes: Φ 9 mm × 1.5 mm) used for *in vivo* and *in vitro* experiments, respectively, were prepared by wire cutting. HA was deposited on the Mg surface using a liquid phase deposition method as described in a previous publication [23]. In the next step, GelMA was dissolved in lithiumphenyl-2,4,6-trimethylbenzoyl phosphinate (LAP) photoinitiator solution at 60 °C–70 °C for about 30 min in the dark, and then GDNF (1 μg, Sino Biological Inc., China) was added to form the GDNF-Gel solution. GDNF-Gel/HA-Mg was then prepared by soaking the HA-coated Mg in the GDNF-Gel solution and was then subjected to 405 nm ultraviolet light.

3.2. Electrochemical measurements

Electrochemical experiments using a three-electrode system were carried out on an electrochemical workstation (Gamry, USA). All the measurements were performed in phosphate-buffered saline (PBS, Service bio, China) at 37 °C. The electrochemical impedance spectroscopy (EIS) signal amplitude was 10 mV over a frequency range of 0.01 Hz–100 kHz. Corrosion potentials (E_{corr}) and corrosion current densities (i_{corr}) were extracted from the potentiodynamic polarization plots using Tafel extrapolation [24]. The impedance spectra were plotted using Nyquist and Bode plots. The fitting of the spectra was analyzed using ZsimpWin 3.6 software and Gamry Echem Analyst. At least three samples were tested for each group.

3.3. Immersion test and hydrogen evolution

All samples were immersed in PBS solution, which was replaced every 24 h, at 37 °C for up to 30 days. The solution volume to sample area ratio was 25 mL/cm^2 in accordance with the ASTM G31-12a standard. The pH and ion concentrations (Mg, Ca) of the solution were measured at the 1st, 3rd, 7th, 15th, and 30th day.

The hydrogen evolution was conducted using the method described in Ref. [25]. An inverted acid burette was used to collect and measure the hydrogen released at the 1st, 3rd, 5th, 10th, 14th, and 28th day. For each group, three samples were measured. The corrosion rate was calculated according to ASTM F3268-18a,

$$P_H = 2.279 V_H$$

V_H = volume (ml)/surface area (cm^2)/days, and P_H = mm/year.

3.4. Surface characterization

The surface microstructure of the samples sputtered with a gold film, was analyzed using an environmental scanning electron microscope (ESEM, Quattro S FEI, USA) equipped with an energy dispersive spectrometer (EDS, Oxford, UK). The characteristic functional groups on the surface of the samples were detected by a Fourier transform infrared spectroscopy (Nicolet iS5, Thermo Fisher Scientific, FTIR) in the wave number range of 500–4000 cm^{-1}. Average surface roughness of the GDNF-Gel/HA-Mg was evaluated using a laser scanning confocal microscopy (OLYMPUS LEXT OLS4000), the laser confocal scan covered an area of 240 μm × 240 μm. At least three profiles were analyzed to obtain average values of the surface roughness. The surface wettability of the samples was investigated by contact angle measurement (Dataphysics Instruments GmbH, OCA20) using a water droplet of 2–3 μL. An inductively coupled plasma-optical emission spectrometer (ICP-OES, Optima 8000 PerkinElmer, USA) was used to analyze the concentrations of Mg and Ca in PBS solution. The pH value of the solution was measured with a pH meter (PHS-3E, Shanghai INESA Scientific Instrument Co.).

3.5. Preparation of extracts

Extracts were prepared by incubating the samples in a Dulbecco's Modified Eagle Medium/Nutrient Mixture F-12 (DMEM/F-12, Shanghai Yuanpei Biotechnology Co., Ltd., China), supplemented with 10 % fetal bovine serum (FBS, NEWZERUM, New Zealand) for 24 h in a humidified atmosphere with 5 % CO_2 at 37 °C. The extraction ratio was 1.25 cm^2/mL in accordance with ISO 10993-1219. The extracts were collected every 24 h, and the supernatant was removed, centrifuged, and kept refrigerated at 4 °C for use within a week.

3.6. Isolation of Schwann cells and live/dead staining

Schwann cells were isolated from Sprague Dawley (SD) rats. The sciatic nerve of SD rats was harvested and minced, then digested with trypsin (InCellGenE, China) and type II collagenase (Sigma-Aldrich, USA) at 37 °C for approximately 1h. The mixture was filtered using a cell strainer (Corning FALCON, USA), and Schwann cells were isolated using a double 30-min differential adhesion method. The isolated cells were cultured at 37 °C with 5 % CO_2 in an incubator (PHCbi, Japan).

Immunofluorescence (IF) was used to identify Schwann cells. To assess the biotoxicity of GDNF-Gel/HA-Mg samples, Schwann cells were cultured with extracts of GDNF-Gel/HA-Mg. Staining was performed at the 1st, 3rd, 5th, and 7th day using the Live&Dead kit (US Everbright® Inc, China).

3.7. Cell cycle, CCK-8 and clone formation assay

Schwann cells with a density of 2×10^5 cells/well were seeded into a 12-well plate. After incubating overnight, the medium was replaced with 100 %, 50 %, and 25 % extracts for high-, medium-, and low-concentration groups, respectively, cells cultured with DMEM/F-12 supplemented with 10 % FBS were selected as control. After 24 h, the cells were then centrifuged (2000 rpm, 5min), washed three times with PBS, fixed overnight with 70 % pre-cooled ethanol. The next day, after washing with PBS, 500 μL of PI/Rnase A working solution (volume ratio of 9:1) (KeyGen BioTECH, China) was added and incubated at room temperature in the dark for 60 min. The cell proportions in the G_0/G_1, S, and G_2/M phases were then detected by flow cytometry (ACEA Biosciences, USA). For CCK-8 assays, 100 μL of Schwann cells suspension containing approximately 5×10^3 cells were seeded in a 96-well plate, 10 μL of CCK-8 solution (Yeasen Biotechnology, China) was added to each well. The plate was incubated in dark for 1 h. After that, the OD values of each well were measured at 450 nm by a microplate reader (Perkinelmer, USA).

Schwann cells were seeded in a 6-well plate at a density of approximately 250 cells/well and cultured with different concentration of extract for 14 days. The cells were stained with 1 % crystal violet (HEART ZBIOLOGICAL TECHNOLOGY CO.LTD., China) and the clone formation rate was calculated.

3.8. Scratch and Transwell assays

Cells were seeded into a 12-well plate at a density of 1×10^5 cells/well and cultured overnight. A 10 μL sterile pipette tip was used to create a vertical line across the wells, cells cultured with DMEM/F-12 were selected as control. After 24 h, the migration of Schwann cells was observed and photographed under a microscope (Motic, USA). A Schwann cell suspension was seeded into the upper chamber of Transwell plates (Corning, USA). Meanwhile, approximately 600 μL of DMEM/F12 containing different concentrations of extracts was added to the lower chamber, with DMEM/F12 alone serving as the control. 24h later, Schwann cells were stained with crystal violet (HEART ZBIOLOGICAL TECHNOLOGY CO.LTD, China) and count under a microscope (Motic, USA).

3.9. Western blotting and enzyme linked immunosorbent assay (ELISA)

Protein was extracted using RIPA lysis buffer (Boster Biological Technology, China), and the total protein concentration was measured using the BCA assay kit (Zhonghui Hecai, China). The protein was loaded onto 10 % SDS-PAGE gel (EpiZyme, China) and electrophoresed at 70 V for 30 min, followed by 120 V for 80 min. Blocked with 5 % defatted milk for 2 h, washed three times with TBST, and incubated with anti-$p75^{NTR}$ (1:2000) (Proteintech, China), Netrin-1 (1:1000, Selleck, USA), Rac1 (1:1000, Selleck, USA), Cdc42 (1:1000, Selleck, USA), UNC5b (1:500, Selleck, USA) antibody overnight at 4 °C. After incubation, the membrane was incubated with goat anti-rabbit IgG H&L (HRP) (1:10000) (Abcam, UK), and then quantified using ECL detection reagent (Vazyme Biotech, China). Additionally, ELISA was employed to measure the levels of NGF.

3.10. Reactive oxygen species (ROS) level and apoptosis

Schwann cells were subjected to oxidative stress-induced cell apoptosis after PNI using H_2O_2 as a stimulant. H_2O_2 was added at a final concentration of 1 mM and incubated for approximately 30 min 1 mL of DCFA-DA (2 μM) (Wanleibio, China) was added and incubated at 37 °C for 20 min, ROS detected by flow cytometry (ACEA Biosciences, USA). For Schwann cell apoptosis detection, Annexin V-FITC and PI staining solution (Elabscience, China) were added into Schwann cell suspension, incubated at room temperature in the dark for 20 min, and analyzed by flow cytometry (ACEA Biosciences, USA).

3.11. Macrophage polarization

RAW264.7 cells were seeded in a 6-well plate with the density of approximately 5×10^5 cells/well and cultured in DMEM/F12 + 10 % FBS overnight. Lipopolysaccharide (final concentration of 1 μg/mL) and IL-4 (final concentration of 20 ng/mL) (Sigma-Aldrich, USA) were added to the routine medium as positive controls for M1 and M2 macrophage polarization, respectively. The cells were incubated with PE anti-mouse CD80 antibody (1:5000; Biolegend, USA), APC anti-mouse CD86 antibody (1:5000; Biolegend, USA), and FITC anti-mouse CD206 antibody (1:5000; Biolegend, USA), the macrophage polarization was analyzed by flow cytometry (ACEA Biosciences, USA).

3.12. Establishment of peripheral nerve defect models

Thiry-two male adult SD rats were randomly divided into three groups: negative control (NC) group, Mg group, GDNF-Gel/HA-Mg group, and Auto group. The rats underwent surgery to expose and excise a portion of the sciatic nerve. In the NC group, the wound was closed without any further treatment. In the Auto group, the excised nerve was sutured back together, and selected as positive control. In the Mg and GDNF-Gel/HA-Mg group, a Mg conduit and GDNF-Gel/HA-Mg conduit were used to connect the nerve ends, respectively.

3.13. HE, Masson and toluidine blue staining

At 12w post-surgery, after anesthesia, rats were sacrificed, the sciatic nerve was perfused with saline and 4 % paraformaldehyde (Servicebio, China). Subsequently, an automatic dehydrator was used for dehydration, and the samples were embedded in paraffin and sectioned. The slides were placed in a hematoxylin solution (Servicebio, China) for staining for 2–3 min, then, the slides were immersed in eosin solution (Servicebio, China). Masson staining was performed as per following steps: dewaxing in xylene, immersion in ethanol solutions of decreasing concentration, rinsing with distilled water, treatment with hematoxylin solution, differentiation with 1 % hydrochloric acid ethanol, exposure to Masson's composite staining reagent. The stained sections were then mounted with neutral gum and observed under a microscope. To evaluate myelinated nerve fibers, regenerated nerve tissues from selected SD rats in each group were obtained 12 weeks post-surgery. The harvested tissues were fixed, dehydrated, embedded for semi-thin sections, stained with toluidine blue. Toluidine blue staining clearly differentiates myelinated and unmyelinated nerve fibers in peripheral nerve sections. Myelinated fibers exhibit a distinctive dark blue, segmented morphology, appearing as regularly spaced "bead-like" structures along axons with typical internodal lengths of 50–80 μm. In contrast, unmyelinated fibers present as faint blue or nearly transparent linear structures without visible myelin wrapping. For quantitative assessment, we implemented a rigorous counting protocol that includes: systematic random selection of 10–20 non-overlapping microscopic fields, differential enumeration of myelinated versus unmyelinated fibers using Image Pro Plussoftware with graphic tablet-assisted manual verification, and calculation of average fiber counts per field.

3.14. Neurophysiology and Gastrocnemius muscle weight assessment

Twelve weeks after surgery, randomly chosen SD rats from each group underwent nerve conduction velocity (NCV) and latency

assessments using the BL-420 Biological Function Experiment System. Following the 12-week mark post-surgery, the animals that underwent neurophysiological evaluations were euthanized. The gastrocnemius muscle was meticulously dissected from the point of origin at the femoral condyles to the distal end at the calcaneal tuberosity, and its wet weight was precisely recorded.

3.15. Statistical analysis

All data are presented as mean ± standard deviation. One-way analysis of variance (ANOVA) was used to compare the statistical differences between groups, LSD test was used for pairwise comparisons. A *P*-value <0.05 was considered statistically significant. All statistical analyses and charts were performed using Graphpad Prism 9.0.

4. Results

4.1. Surface morphology and property of GDNF-Gel/HA-Mg

HA-Mg was prepared by liquid phase deposition. Under examination with a scanning electron microscope (SEM), the surface revealed small fluffy spherical particles of HA-Mg that exhibited an even distribution across the material surface, consistent with the microstructure of HA particles (Fig. S1). An analysis performed using Energy-dispersive X-ray spectroscopy (EDS) on the surface scan of HA-Mg identified a uniform distribution of elements including C, Ca, Mg, Na, O, P throughout the material surface (Fig. S1). Using photopolymerization, different concentrations of GDNF-Gel gel (5 %, 10 %, and 15 %) were successfully synthesized. The GDNF-Gel gel displayed excellent swelling properties and sustained release of GDNF (Fig. S2). Notably, the 10 % concentration of GDNF-Gel showed superior effects in promoting cell proliferation, as observed in the CCK-8 assay (Fig. S2). Consequently, the 10 % GDNF-Gel was chosen for further experiments. The microstructure of the

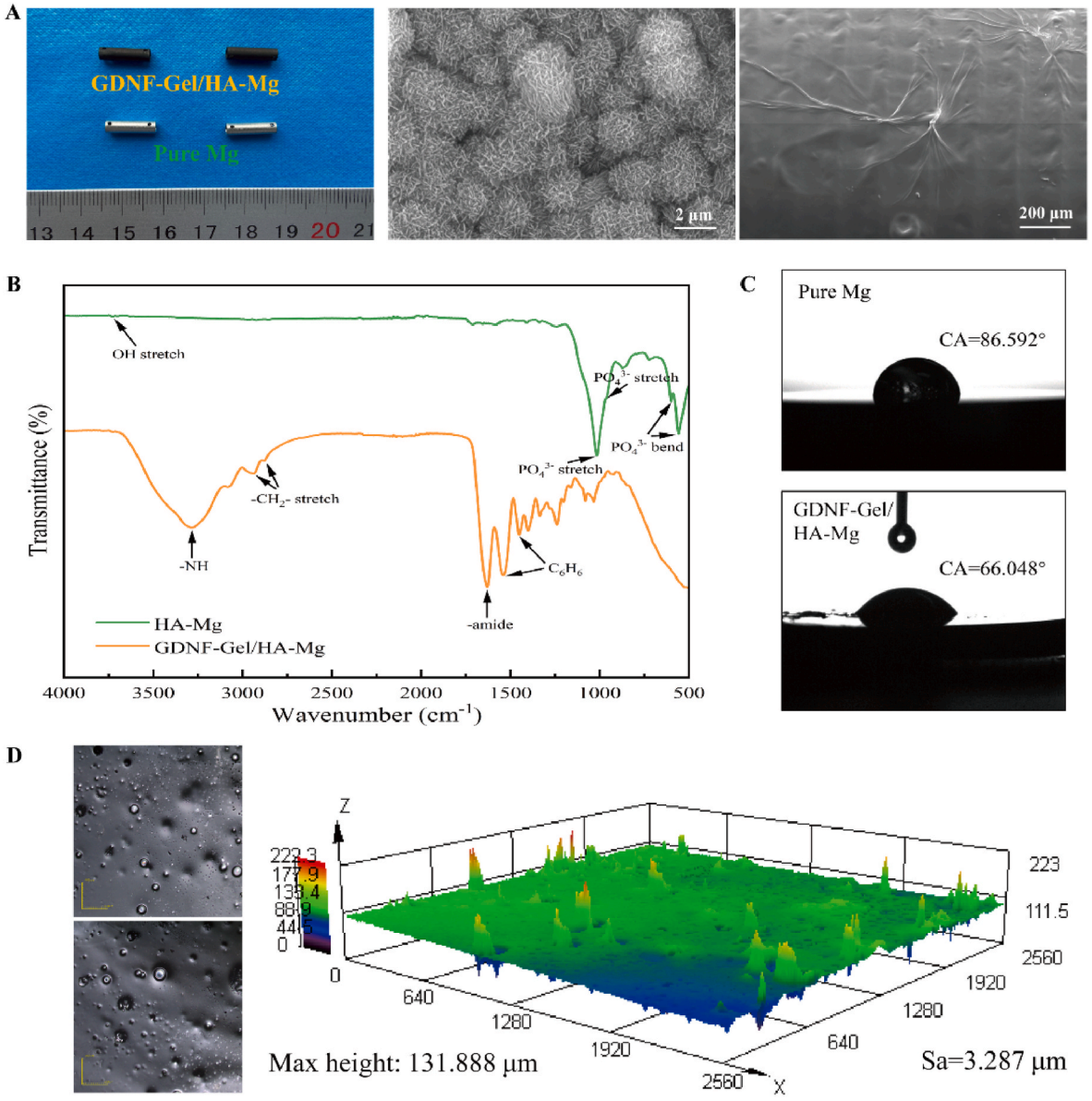

Fig. 2. Preparation and characterization of GDNF-Gel/HA-Mg material. A: The surface morphologies of pure Mg and GDNF-Gel/HA-Mg; B: FTIR spectrum of HA-Mg and GDNF-Gel/HA-Mg; C: The surface wettability of pure Mg and GDNF-Gel/HA-Mg; D: The surface roughness of GDNF-Gel/HA-Mg. Mg: magnesium; HA: hydroxylapatite; GDNF: glial cell line-derived neurotrophic factor; GelMA: Gelatin methacryloyl.

10 % GDNF-Gel hydrogel was observed by SEM, and the results revealed a porous architecture (Fig. S2). The pores exhibited variability in size but were evenly distributed, which created an optimal environment for cell attachment. The porous structure also contributed to the storage and controlled release of GDNF, enabling the maintenance of GDNF concentration in local tissues and ultimately enhancing therapeutic effectiveness. Furthermore, after being labelled by Cy5.5, small animal *in vivo* imaging demonstrated that the 10 % GDNF-Gel hydrogel exhibited a degradation time of approximately 50 days (Fig. S2).

The topographies of GDNF-Gel/HA-Mg, engineered with precisely controlled hierarchical architecture through a sequential fabrication protocol, were shown in Fig. 2A, with an inner matrix consisting of spherical HA-Mg particulate clusters, and an outer functional layer of GDNF-incorporated hydrogel (GDNF-Gel). Fig. 2B showed the result of the FTIR experiment. The $\nu 4$ doubly degenerate asymmetric OP-O bending mode of the PO_4^{3-} tetrahedron was identified by two peaks at 558 and 600 cm^{-1}. The peaks detected at 960 and 1014 cm^{-1} were attributed to the triply degenerate asymmetric P-O stretching mode of the PO_4 group. The peak at 3724 cm^{-1} resulted from the hydroxyl stretching vibration of HA [26]. The absorption peaks detected at 1450 and 1537 cm^{-1} were characteristic of C_6H_6, while the peak at 1630 cm^{-1} indicated the presence of amide, suggesting that the main network in the hydrogel consisted of polyacrylamide, which could be from the photo-crosslinking process of GDNF-Gel [27]. The characteristic absorption peaks of the asymmetric and symmetric stretching of methylene were detected at 2879 and 2937 cm^{-1}, respectively, and the characteristic absorption peak of related -NH peak at 3280 cm^{-1}. These results confirmed the existence of the HA and GDNF-Gel coatings.

Fig. 2C illustrated that on the pure Mg surface, the contact angle was 86.59°, whereas on the GDNF-Gel/HA-Mg surface, it decreased to 66.05°. The increase in hydrophilicity could be attributed to the presence of hydrophilic functional groups in the coating. Fig. 2D displayed the 3D roughness of the GDNF-Gel/HA-Mg. Micro-pores and irregularities were formed on the sample surface. Although the local maximum height difference is 131.89 μm, the overall surface roughness is only 3.29 μm. This agreed with the SEM images in Fig. 2A.

4.2. Corrosion resistance of GDNF-Gel/HA-Mg in PBS solution

As depicted in Fig. 3A, the E_{corr}s of pure Mg, HA-Mg, and GDNF-Gel/HA-Mg in PBS were −1.75 V, −1.63 V, and −1.58 V, respectively, and the i_{corr}s were 2.62×10^{-5} A cm^{-2}, 3.04×10^{-6} A cm^{-2}, and 2.42×10^{-6} A cm^{-2}, respectively. The i_{corr} of GDNF-Gel/HA-Mg decreased and the E_{corr} increased compared to pure Mg. On the other hand, the radius of the semicircle corresponding to GDNF-Gel/HA-Mg (with an impedance value of 5.41×10^3 Ω cm^{-2}) was larger than that of HA-Mg (with an impedance value of 4.87×10^3 Ω cm^{-2}) and pure Mg (with an impedance value of 1.02×10^3 Ω cm^{-2}) (Fig. 3B), the expansion in the diameter of the Nyquist plot indicates an elevated corrosion resistance of the coated Mg [28]. The Bode plot revealed the presence of two relaxation time constants, discernible through the two peaks in the phase angle plot. The peaks in the high-frequency range between 1 Hz to 10^5 Hz were apparent, however those in the medium to low-frequency range (0.01–1 Hz) were inconspicuous which was affected by the corrosion of Mg substrate and coating (Fig. 3C) [29]. In addition, HA-Mg showed a maximum phase angle of −65.89°, whereas GDNF-Gel/HA-Mg and pure Mg display showed lower maximum phase angles of −56.68° and −57.74° respectively (Fig. 3C). Nevertheless, GDNF-Gel/HA-Mg consistently demonstrates a higher phase angle than that of HA-Mg and pure Mg in the medium to low-frequency range, thereby indicating a heightened corrosion resistance, attributable to its elevated absolute maximum phase angle.

Fig. 3D–F showed the variations of the △pH values and ion concentrations of PBS during the immersion period. △pH of PBS with pure Mg was 0.85 at the fifth day and then decreased to around 0.56 till the end of immersion. The PBS immersed with coated samples taken 30 days to reach the △pH value similar to those of the pure Mg group (Fig. 3D). This phenomenon demonstrated that the calcium phosphate coatings provide effective protection to Mg at the initial stage of corrosion. The Mg^{2+} and Ca^{2+} release curves showed an improvement in the corrosion resistance of GDNF-Gel/HA-Mg compared to the other samples. The Mg^{2+} concentration in PBS with pure Mg was very high (25.78 mg/L) in the first 7 days of immersion, and then dropped to 14.38 mg/L on day 30

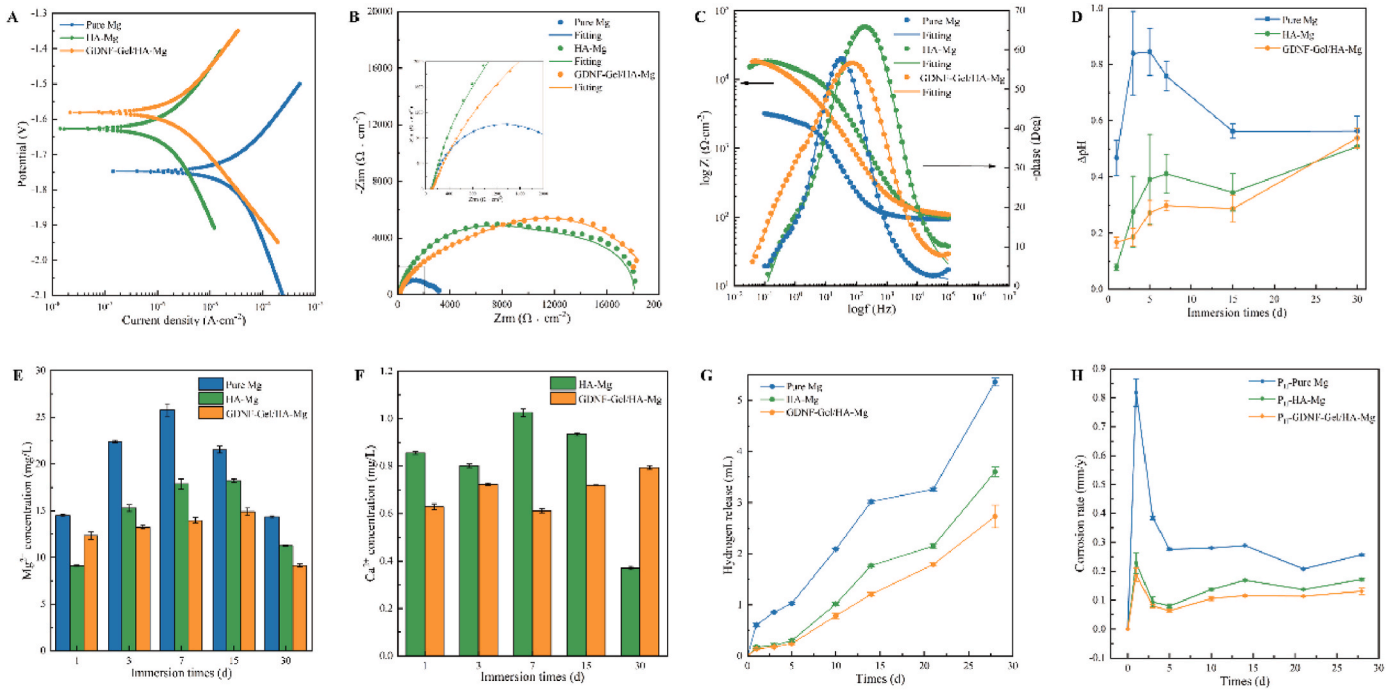

Fig. 3. The corrosion resistance of GDNF-Gel/HA-Mg in PBS solution using various test methods. A: Potentiodynamic polarization curves; B: electrochemical impedance spectroscopy curves; C: Bode plot; D: △pH values in PBS; E: Mg^{2+} concentrations in PBS; F: Ca^{2+} concentrations in PBS; G: Hydrogen evaluation; H: Corrosion rate. Mg: magnesium; HA: hydroxylapatite; GDNF: glial cell line-derived neurotrophic factor; GelMA: Gelatin methacryloyl.

(Fig. 3E). In contrast, the Mg^{2+} concentration was suppressed by the HA and GDNF-Gel coatings, the Mg^{2+} concentration with coated samples both need a longer time (15 days) to reach the highest value (18.21 mg/L for HA-Mg, and 14.91 mg/L for GDNF-Gel/HA-Mg) (Fig. 3E). As for the Ca^{2+} concentration, GDNF-Gel/HA-Mg showed a biphasic profile, which slightly increased to 0.72 mg/L in the first 3 days, followed by a dramatic decrease to 0.61 mg/L until day 7, which afterward elevated to 0.79 mg/L in the end (Fig. 3F). The Ca^{2+} release rate was suppressed by GDNF-Gel coating compared with HA-Mg, especially in the first 15 days of immersion corrosion.

The hydrogen evolution of the samples in PBS solution was displayed in Fig. 3G. The H_2 generation of all three samples kept increasing with immersion time. At the initial stage, the hydrogen gas evolved was maximum from the surface of pure Mg. The HA-Mg and GDNF-Gel/HA-Mg samples exhibited a small volume of evolved hydrogen in the first 5 days, and then appeared a rapid increase from the range of 0.24–0.3 mL to 2.73–3.6 mL (Fig. 3G). During the whole immersion, the evolved hydrogen for GDNF-Gel/HA-Mg was slightly lower than that of HA-Mg (Fig. 3G). The corrosion rate calculated from the hydrogen evolution also confirmed the difference in corrosion resistance of the various samples. All the samples exhibited a drastic decrease in corrosion rate from 1 to 5 days, followed by a slight increase from 5 to 15 days, which afterward remained at a low level from 15 to 28 days. On the first day post immersion, as compared to the high corrosion rate of pure Mg of 0.82 mm/y, for HA-Mg it was 0.23 mm/y, and for GDNF-Gel/HA-Mg was 0.19 mm/y, which corresponds to a marked decrease by 71.95 % and 76.83 %, respectively (Fig. 3H). Over the next few days, GDNF-Gel/HA-Mg maintained a steady, and the slowest release profile with a calculated corrosion rate of 0.13 mm/y on day 28, which represented a considerable enhancement of corrosion resistance by 23.53 % and 50 % compared to HA-Mg and pure Mg, respectively (Fig. 3H). The results suggested that GDNF-Gel/HA-Mg improved the corrosion resistance of pure Mg in PBS solution, which was in accordance with the results obtained from the electrochemical and immersion tests.

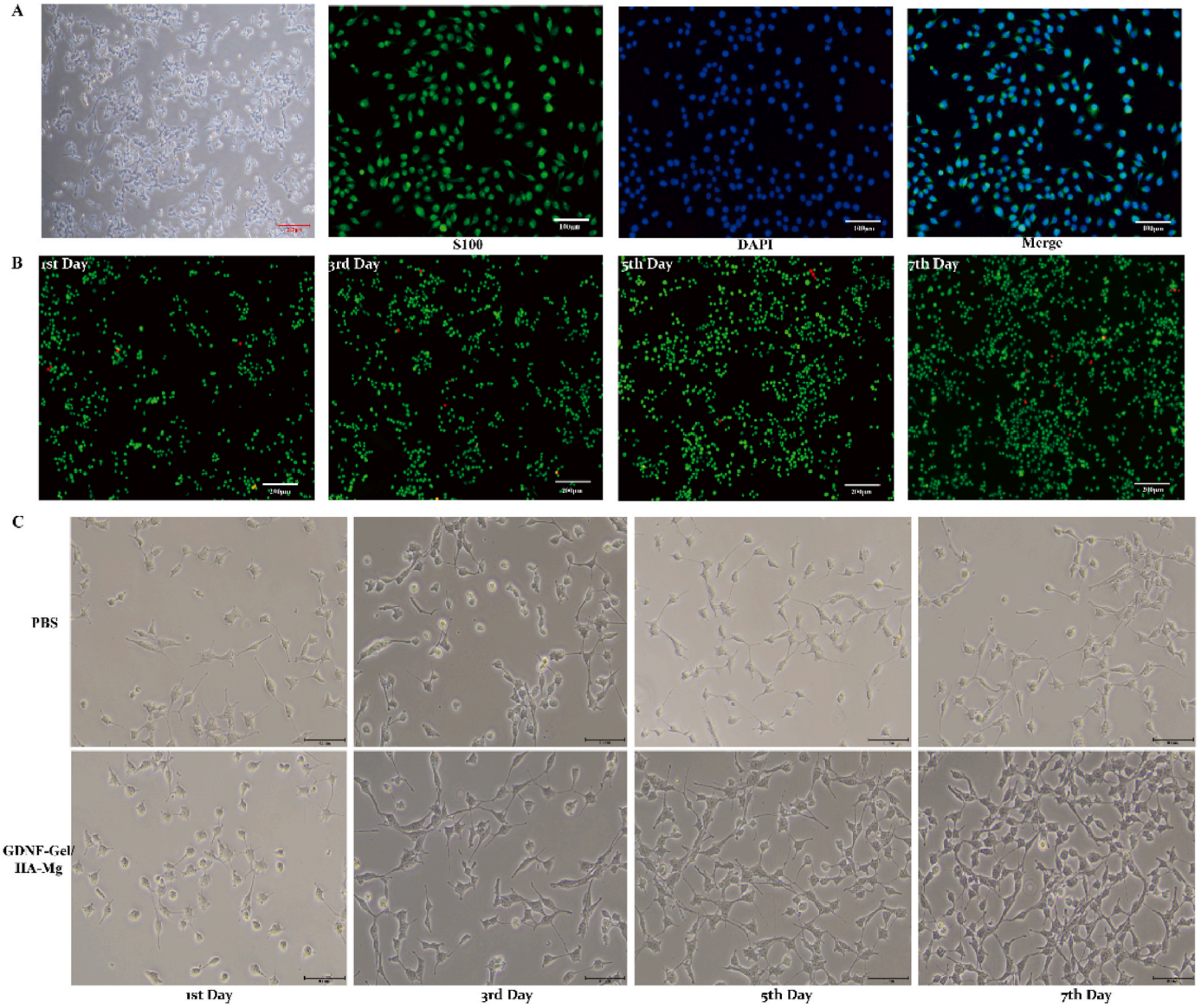

Fig. 4. Isolation and identification of Schwann cells, biocompatibility assessment. A: Microscopic morphology of isolated Schwann cells and identified by immunofluorescence; B: Live/Dead staining was performed after GDNF-Gel/HA-Mg extracts were co-cultured with Schwann cells for 1, 3, 5 and 7 days, which showed good biocompatibility; C: Microscopic morphology of Schwann cells after being cultured with extracts.

4.3. GDNF-Gel/HA-Mg exhibits favorable biocompatibility with Schwann cells

Schwann cells and fibroblasts from SD rat sciatic nerves were separated using a double 30-min differential adhesion method. The isolated cells presented distinct protrusions from the cell body under the microscope, extending two long antennae in a spindle shape or three antennae in a triangular shape, which is consistent with the microscopic morphological characteristics of Schwann cells (Fig. 4A). The identity of these cells was further confirmed as Schwann cells by conducting IF targeting the S100, a known Schwann cell marker (Fig. 4A). Cell adhesion tests demonstrated that numerous Schwann cells were found to adhere to the HA-Mg surface, in contrast to the visibly lesser amount adhered to the Mg surface. This indicates that HA-Mg demonstrated a notable advantage in Schwann cells adhesion, with its exceptional Schwann cells adhesion capabilities providing strong support for nerve tissue regeneration (Fig. S3).

After 1, 3, 5, and 7 days of co-culture with GDNF-Gel/HA-Mg extracts (100 %), live/dead staining was performed on Schwann cell for biocompatibility assessment, with live cells appearing green and dead cells appearing red, the results showed that GDNF-Gel/HA-Mg extracts did not exhibit any notable cytotoxic effects, suggesting a good biocompatibility (Fig. 4B). During the co-cultivation, we also observed significant morphological changes in the Schwann cells. Initially, on the 1st day, the cell bodies of Schwann cells appeared round or triangular, with short and sparse protrusions. However, as the co-cultivation progressed, there was a gradual transformation in the morphology of Schwann cells, characterized by a notable increase in both the number and length of protrusions, with enhanced extension (Fig. 4C). In the later stages of co-cultivation, Schwann cells began to form clusters, arranging themselves end-to-end or side-by-side. Dense neural networks formed between the protrusions, displaying a pattern reminiscent of a vortex or fence-like formation, similar to the Büngner bands seen in the *in vivo* following nerve injury, which plays a crucial role in nerve regeneration (Fig. 4C). This suggested that GDNF-Gel/HA-Mg extracts not only demonstrated excellent biocompatibility but also stimulates changes in Schwann cells' morphology, particularly in promoting the growth and extension of protrusions.

4.4. GDNF-Gel/HA-Mg promotes Schwann cell proliferation

In order to investigate the impact of GDNF-Gel/HA-Mg extracts on Schwann cell proliferation, cell cycle, clone formation, and CCK-8 assays were performed. As depicted in Fig. 5AC, a notable increased S phase Schwann cells were observed ($P < 0.05$) after cultured with high-concentration of extracts for 24h, while no significant changes in the number of G_0/G_1 and G_2/M phase cells. The clone formation rate increased progressively when cultured in medium- and high-concentration of extracts (Fig. 5BD). Furthermore, the CCK-8 assays also indicated that culturing Schwann cells with medium- and high-concentration of extracts could promote the proliferation of Schwann cells (Fig. 5E).

4.5. GDNF-Gel/HA-Mg increases Schwann cell migration ability

The GDNF-Gel/HA-Mg extracts were prepared by serum-free

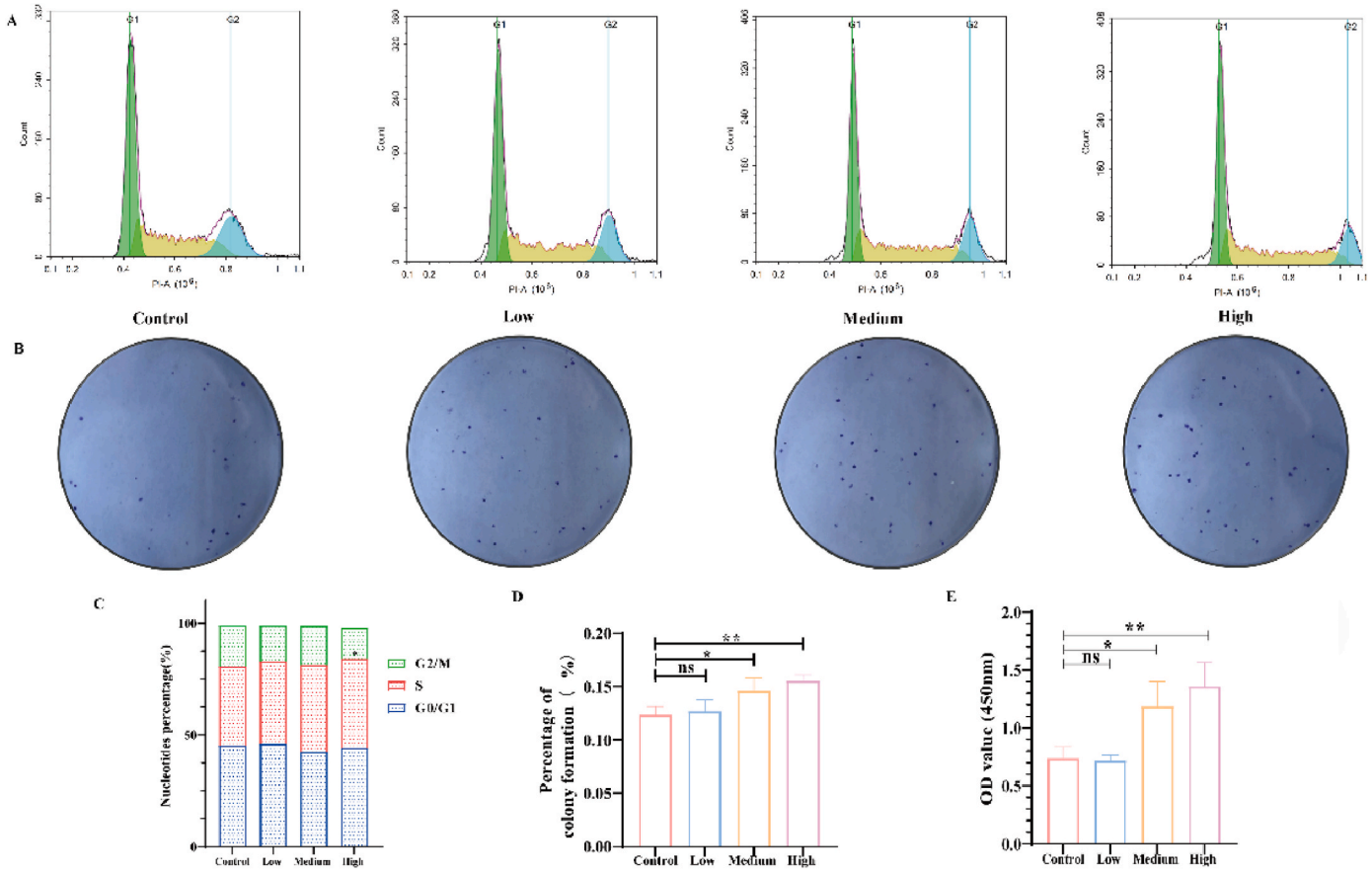

Fig. 5. The effect of different concentrations of extracts on the proliferation of Schwann cells. A, C: Detection and analysis of the number of Schwann cells in G_0/G_1, S, and G_2/M phases after co-culture with different concentrations of extracts by flow cytometry; B, D: The effect of different concentrations of extracts on the clone formation of Schwann cells; E: Assessment of the effect of different concentrations of extracts on the proliferation of Schwann cells by CCK-8 assay. OD: optical density; ns: no statistical significance; $^*P < 0.05$; $^{**}P < 0.01$.

DMEM/F12 in this experiment to assess the effect on Schwann cell migration ability. The scratch assays findings indicated that when culture with low- and medium-concentration of extracts, there were no significant change in Schwann cell migration ability, while high-concentration of extracts could improve the migration ability of Schwann cells to a certain degree (Fig. 6A–C). Moreover, the effect of GDNF-Gel/HA-Mg extracts on Schwann cells migration ability was also investigated by Transwell assays (Fig. 6D). The results revealed that Schwann cells migration ability did not change when low-concentration of extract was added to the lower chamber, but medium- and high-concentration of extracts could significantly increase the Schwann cells migration ability in a dose-dependent manner (Fig. 6EF).

4.6. GDNF-Gel/HA-Mg reduces Schwann cell ROS levels and apoptosis

In this experiment, H_2O_2 were used to stimulate Schwann cells, mimicking the oxidative stress environment following PNI, and the effect of GDNF-Gel/HA-Mg extracts on Schwann cell ROS levels and apoptosis were further investigated. As shown in Fig. 7, the intracellular ROS levels in Schwann cells increased significantly after H_2O_2 was added, while cultured with the extracts led to a significant reduction in the intracellular ROS levels in a dose-dependent manner (Fig. 7 AC).

Additionally, extensive Schwann cell apoptosis was resulted from H_2O_2 stimulation, however, upon cultured with varying concentration of extracts, it was observed that the H_2O_2 -induced Schwann cell apoptosis, including early and late apoptosis, was significantly reduced as the concentration of extracts increased (Fig. 7 BD).

These findings suggest that GDNF-Gel/HA-Mg might protect Schwann cells from apoptosis caused by oxidative stress after PNI.

4.7. GDNF-Gel/HA-Mg promotes the expression of genes related to nerve regeneration

The NGF concentration in the supernatant and the expression of $p75^{NTR}$ at protein level in Schwann cells were detected. The results showed that as the concentration of the extracts increased, the NGF secreted by Schwann cells in the supernatant gradually increased (Fig. 8A). Moreover, the Western blotting and IF results revealed that after cultured with medium- and high-concentration of extracts, the expression level of $p75^{NTR}$ significantly increased in a dose-dependent manner (Fig. 8B–E). To delve deeper into the mechanisms by which GDNF-Gel/HA-Mg promotes the proliferation and migration of SCs, we conducted further analysis on key genes involved in these processes. Results depicted in Fig. 8F–I demonstrate that, in comparison to the control group, the expression levels of genes associated with axonal regeneration and autophagy in Schwann cells, such as Netrin-1, exhibited a gradual increase with escalating concentrations of the extract. This increase was particularly notable in cultures with medium- and high-concentration of

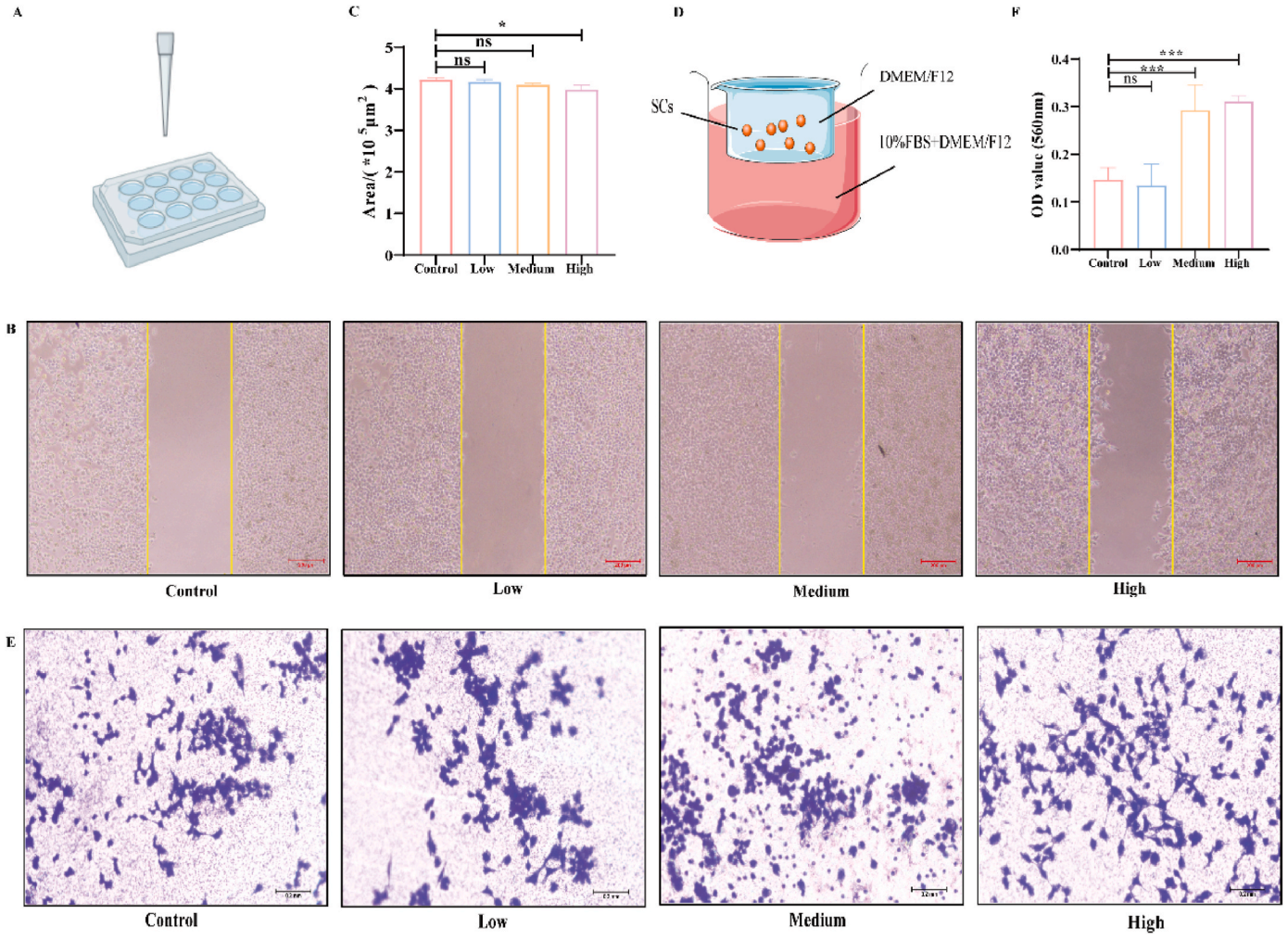

Fig. 6. The effect of different concentrations of extracts on Schwann cells migration ability. A: Schematic diagram of the cell scratch assay; BC: The effects of different dose extracts on Schwann cells migration ability assessed by scratch assays and statistical analysis; D: Schematic diagram of the Transwell assay; E–F: The effects of different dose extracts on Schwann cells migration ability as measured by Transwell assay and statistical analysis. SCs: Schwann cells; FBS: Fetal bovine serum; ns: no statistical significance; $^*P < 0.05$; $^{***}P < 0.001$.

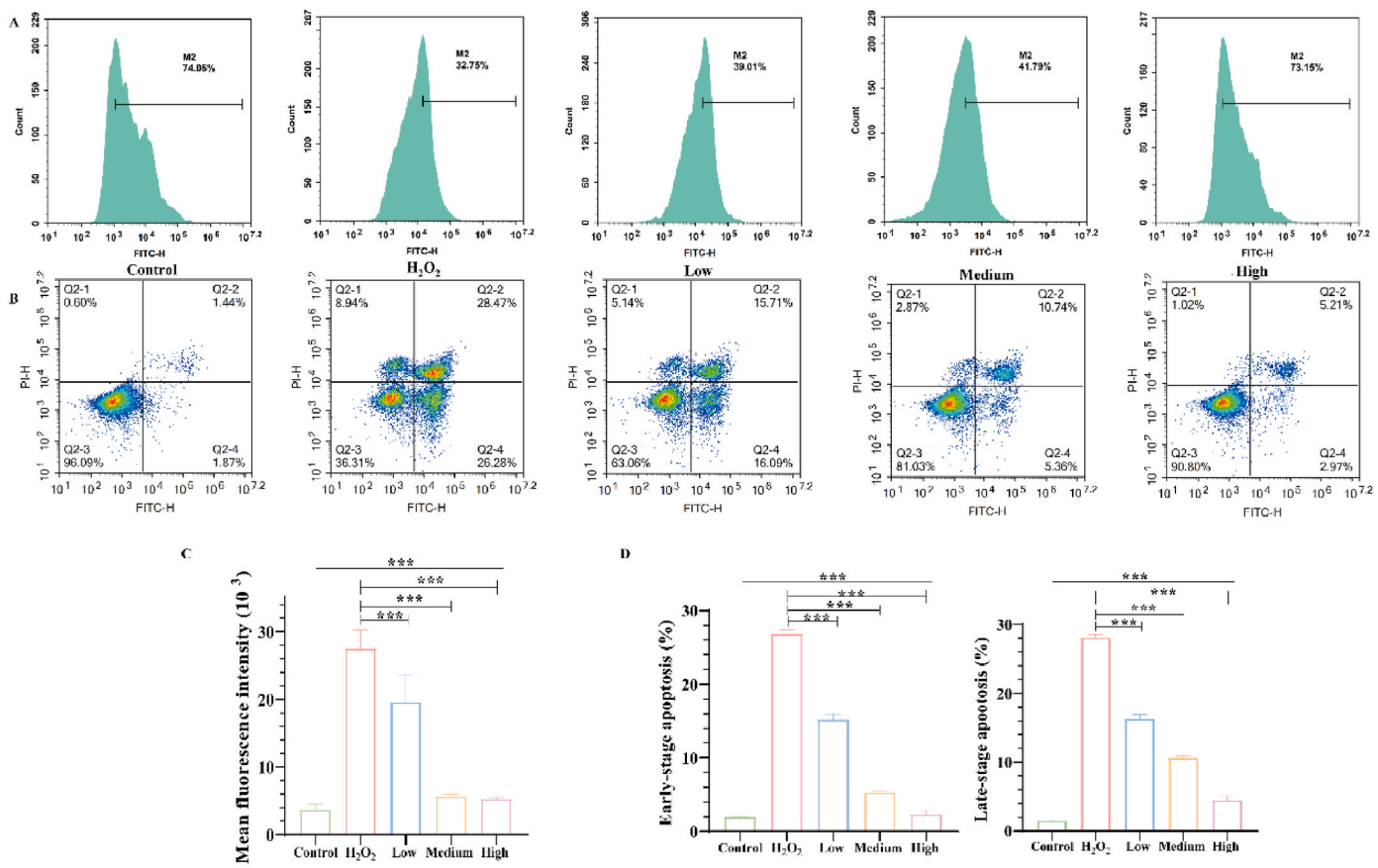

Fig. 7. The effect of different concentrations of extracts on H_2O_2-induced reactive oxygen species (ROS) levels and cell apoptosis in Schwann cells. A, C: the effect of different concentrations of extracts on H_2O_2-induced ROS levels detected by flow cytometry and statistical analysis; B, D: the effect of different concentrations of extracts on Schwann cell apoptosis detected by flow cytometry and statistical analysis. $^{***}P < 0.001$.

extracts, resulting in a significant elevation in Netrin-1 protein expression. Moreover, following cultured with medium- and high-concentration of extract, there was a marked increase in the protein expression levels of Rac1 and Cdc42, which are pivotal for Schwann cells migration. Remarkably, in the high-concentration group, the expression of Cdc42 was notably higher compared to the medium concentration group, while there was no significant disparity in the expression levels of Rac1 between the medium- and high-concentration groups. Finally, our assessment also extended to the evaluation of UNC5b receptor expression, which is associated with Schwann cells proliferation. We found that the GDNF-Gel/HA-Mg extract significantly boosted UNC5b protein expression. Notably, this enhancement was not contingent on extract concentration.

4.8. GDNF-Gel/HA-Mg facilitates M2 macrophage polarization

During the progression of tissue inflammation, M1 macrophages appear in the initial stage, recruiting numerous inflammatory cells and exerting pro-inflammatory effects. These macrophages then polarized to the M2 macrophages under certain cytokine stimulation, which consequently inhibits the recruitment of inflammatory cells, marking an anti-inflammatory response. Simultaneously, M2 macrophages could promote angiogenesis and tissue repair. Hence, the influence of GDNF-Gel/HA-Mg extracts on the polarization process of macrophages were further examined. The results indicated that with the increase in the concentration of the extracts, the number of $CD86^+$ and $CD80^+$ macrophages decreased, namely, the M1 macrophages polarization is gradually suppressed (Fig. 9AB); while the number of $CD206^+$ macrophages increased, indicating that the extracts could significantly promote the M2 macrophages polarization in a dose-dependent manner (Fig. 9C).

4.9. GDNF-Gel/HA-Mg conduit promotes sciatic nerve regeneration

To further investigate the role of GDNF-Gel/HA-Mg in repairing sciatic nerve defects, we created an SD rat model and conducted *in vivo* experiments. HE staining results revealed that the NC and Mg groups exhibited disorganized and sparse nerve fiber arrangements, with more connective tissue present (Fig. 10A). In contrast, the Auto and GDNF-Gel/HA-Mg groups showed neatly arranged and densely packed nerve fibers, forming a parallel and wavy structure. The regenerating axons were evenly distributed, and there was no disorganized fiber tissue (Fig. 10A). Masson staining revealed distinct tissue composition patterns across groups (Fig. 10B). In the NC group, dense collagen fiber deposition (stained blue) with irregular morphology predominated, exhibiting characteristic wavy, disorganized bundles indicative of fibrotic scarring, while regenerating nerve fibers (stained red) were sparsely distributed. The Mg group demonstrated increased red-stained neural tissue compared to NC, though persistent blue collagen fibers maintained relatively disordered spatial arrangements—a pattern suggestive of incomplete fibrotic resolution. Strikingly, both Auto and GDNF-Gel/HA-Mg groups displayed robust regeneration evidenced by: predominant red-stained nerve fibers with parallel alignment, significantly reduced blue collagen signals, and histological architecture resembling native endoneurial organization. These results suggest that the use of GDNF-Gel/HA-Mg nerve conduits in repairing sciatic nerve defects could facilitate the regeneration and organized arrangement of nerve fibers, reduce collagen fiber deposition, minimize scar tissue formation and collagen fiber blockage, and ultimately improve the efficacy of nerve repair.

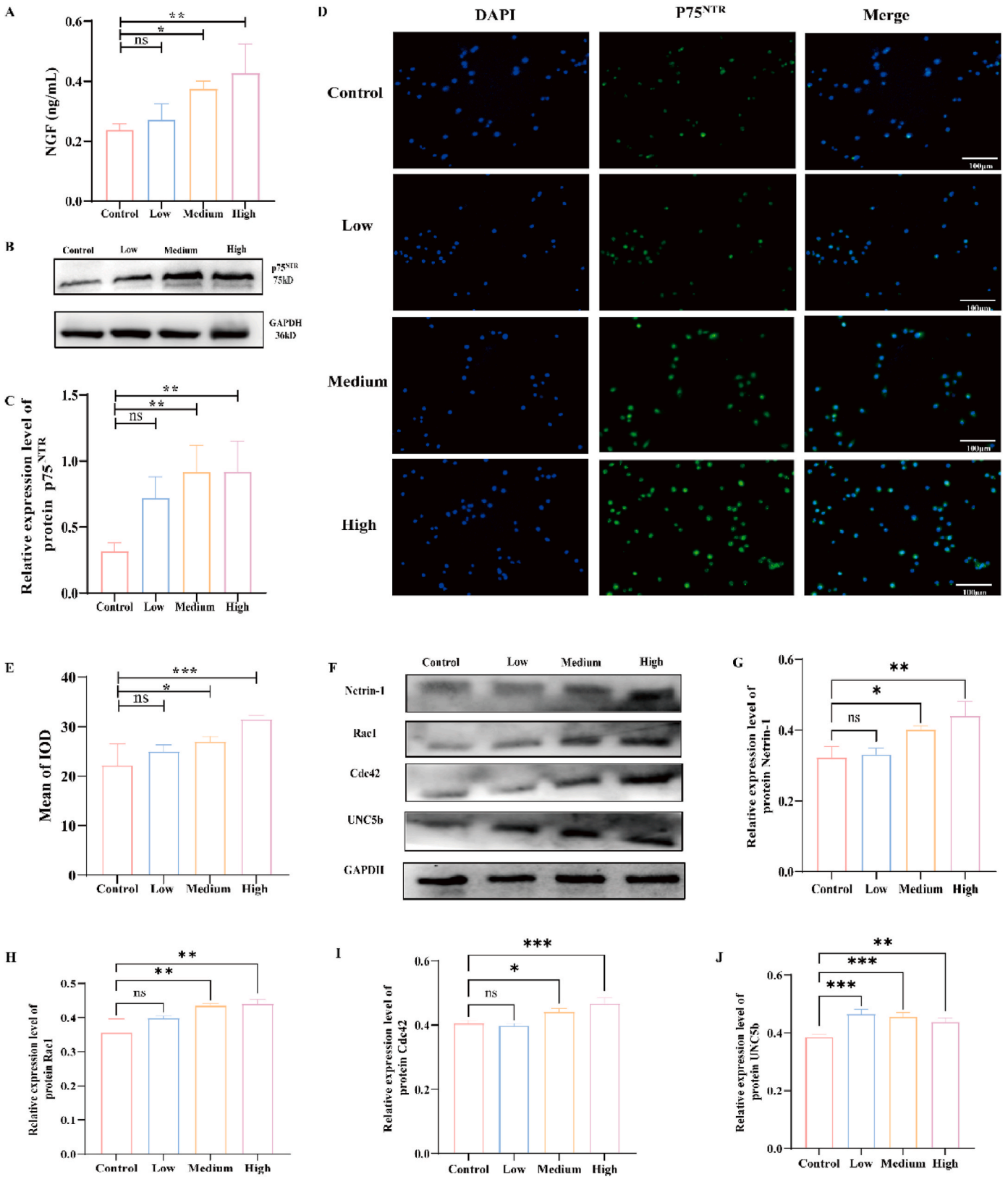

Fig. 8. GDNF-Gel/HA-Mg extracts on NGF secretion, $p75^{NTR}$ and Schwann cell proliferation, migration related genes expression. A: ELISA was used to detect the concentration of NGF in the supernatant. BC: The effect of different concentrations of extracts on the expression level of the p75NTR in Schwann cells detected by western blotting and statistical analysis; DE: The effect of different concentrations of extracts on the expression level of the p75NTR in Schwann cells detected by immunofluorescence and statistical analysis; F–J: the expression of Netrin-1, Rac1, Cdc42 and UNC5b in Schwann cells detected by western blotting and statistical analysis. NGF: nerve growth factor; $p75^{NTR}$: p75 neurotrophin receptor; IOD: integrated optical density; ns: no statistical significance; $^{*}P < 0.05$; $^{**}P < 0.01$; $^{***}P < 0.001$.

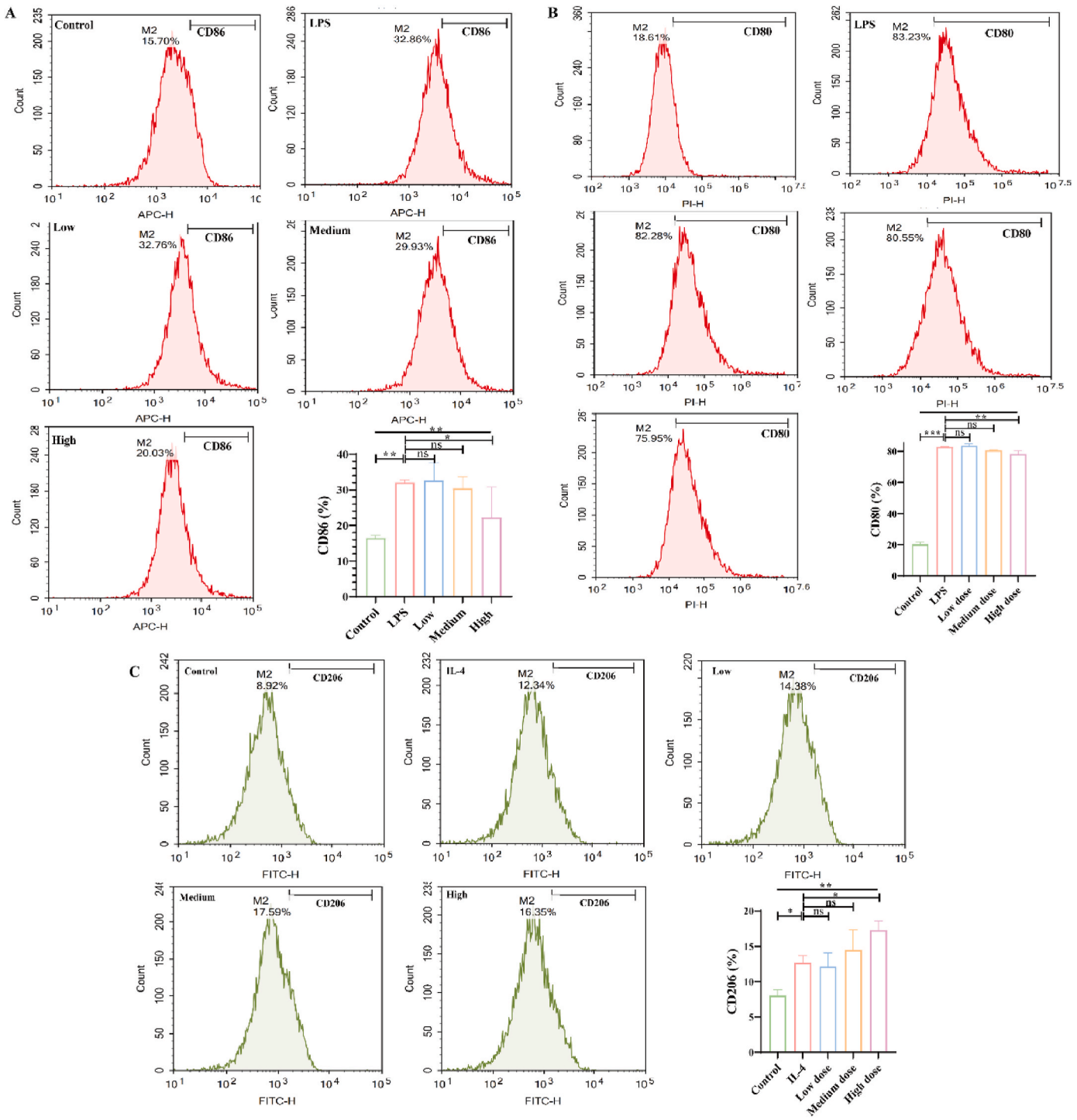

Fig. 9. The effect of GDNF-Gel/HA-Mg extracts on macrophage polarization. AB: Flow cytometry detection of M1 macrophage polarization markers CD86 (A) and CD80 (B) in RAW264.7 macrophages, and statistical analysis; C: Flow cytometry detection of M2 macrophage polarization marker CD206 in RAW264.7 macrophages and statistical analysis. LPS: lipopolysaccharide; IL-4: Interleukin-4; ns: no statistical significance; $^{*}P < 0.05$; $^{**}P < 0.01$; $^{***}P < 0.001$.

4.10. GDNF-Gel/HA-Mg conduit facilitates myelination of regenerated nerve

The nerve electrophysiology test results revealed that both the GDNF-Gel/HA-Mg and Auto groups exhibited shorter latency periods and faster conduction velocities compared to the NC group (Fig. 10CD). Additionally, the toluidine blue staining results illustrated in Fig. 11 AB indicated that there was no notable difference in the number of myelinated nerve fibers between the Mg group and the NC group ($P > 0.05$). However, the GDNF-Gel/HA-Mg and Auto group displayed a considerably higher number of myelinated nerve fibers than the NC group ($P < 0.001$). Furthermore, the Auto group demonstrated a greater number of myelinated nerve fibers when compared to the GDNF-Gel/HA-Mg group ($P < 0.05$).

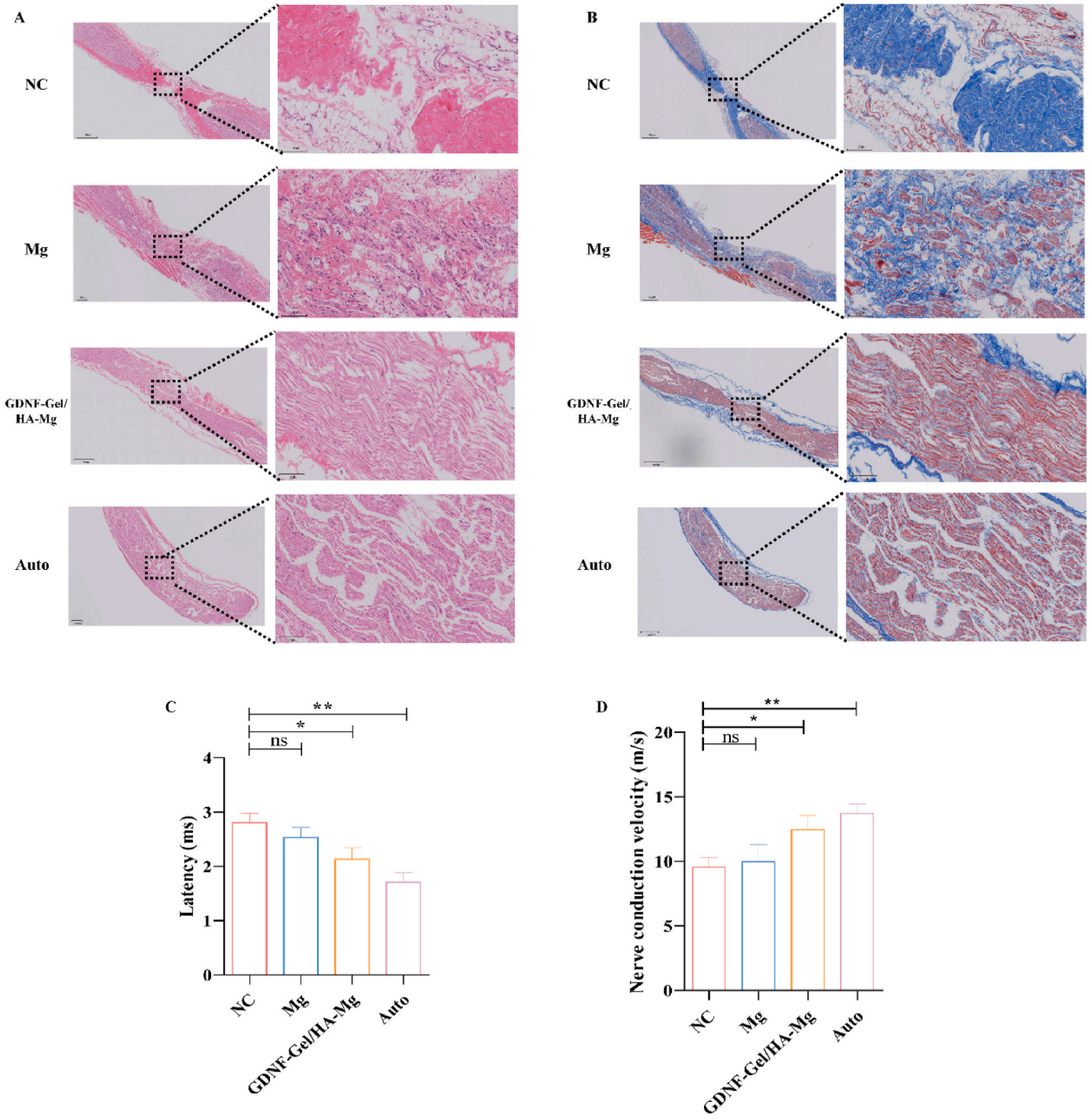

Fig. 10. GDNF-Gel/HA-Mg conduit on sciatic nerve regeneration. A: HE staining results of regenerated sciatic nerves; B: Masson staining results of regenerated sciatic nerves; CD: The latency and nerve conduction velocity of sciatic nerves in different groups. Mg: magnesium; HA: hydroxylapatite; GDNF: glial cell line-derived neurotrophic factor; GelMA: Gelatin methacryloyl. ns: no statistical significance; $^{*}P < 0.05$; $^{**}P < 0.01$.

4.11. GDNF-Gel/HA-Mg conduit promotes nerve regeneration-related gene expression and prevention of gastrocnemius atrophy

The IF showed that the expression of $p75^{NTR}$ in the GDNF-Gel/HA-Mg and Auto group were significantly higher than that of NC and Mg group (Fig. 11CD). In the 12th week of the experiment, the gastrocnemius muscles were removed and subjected to macroscopic observation and comparison to analyze the changes in muscle morphology and size. Upon direct visual observation, it was noted that the NC group exhibited more pronounced atrophy of the soleus muscle (Fig. 11E), attributed to muscle deterioration resulting from nerve damage and subsequent loss of nerve supply. In contrast, the GDNF-Gel/HA-Mg group and Auto group showed larger diameters of the soleus muscle compared to the NC group, with significantly higher wet weights (Fig. 11EF). Importantly, the Mg group also demonstrated a notably higher soleus muscle weight than the NC group ($P < 0.05$), potentially due to the conductivity of Mg providing some level of electrical stimulation to muscles innervated by the distal end, thereby aiding in the recovery of gastrocnemius muscles atrophy caused by denervation. These experimental findings indicated that the GDNF-Gel/HA-Mg nerve conduit not only exhibited effective

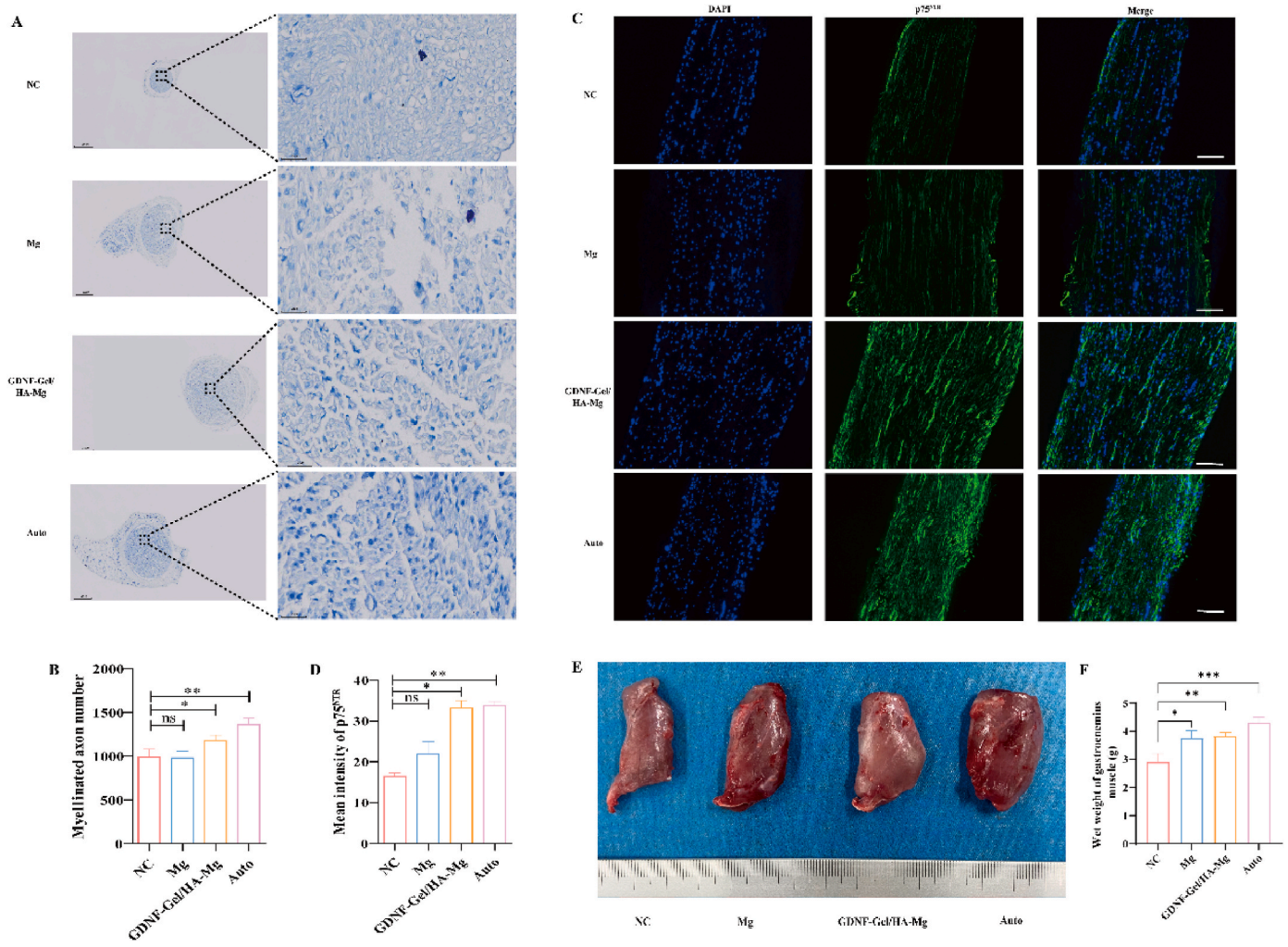

Fig. 11. The effect of GDNF-Gel/HA-Mg conduit on myelination of regenerated sciatic nerves and prevention of gastrocnemius muscle atrophy. AB: Toluidine blue staining results of sciatic nerves in different groups and statistical analysis; CD: The expression of $p75^{NTR}$ detected by immunofluorescence and statistical analysis; EF: The morphologies of gastrocnemius muscle in different groups and statistical analysis. Mg: magnesium; HA: hydroxylapatite; GDNF: glial cell line-derived neurotrophic factor; GelMA: Gelatin methacryloyl; $p75^{NTR}$: p75 neurotrophin receptor. ns: no statistical significance; $^{*}P < 0.05$; $^{**}P < 0.01$; $^{***}P < 0.001$. (For interpretation of the references to color in this figure legend, the reader is referred to the Web version of this article.)

performance in promoting nerve regeneration but also played a significant role in the prevention of muscle atrophy.

5. Discussion

To our knowledge, there were limited studies about the use of Mg alloys in peripheral nerve regeneration. Li et al. [22] used Mg wire to bridge the injured nerve in an acute sciatic nerve compression injury model, the findings showed that the Mg group exhibited an increase in sciatic functional index (SFI), nerve growth factor (NGF), $p75^{NTR}$, and tyrosine receptor kinase A expression after 4 weeks. However, the repair outcome differs depending on the length of the gap [30]. Almansoori et al. [31] found that HA-WE43 promoted the adhesion and proliferation of pheochromocytoma cells (PC12), but its effect on Schwann cells was not significant, although *in vivo* experiments indicated that HA-WE43 could slow down the degradation of magnesium and decrease hydrogen production during degradation, its ability to improve the repair of the sciatic nerve was limited. Therefore, optimization of magnesium-based conduit to increase its corrosion, degradation rate and bioactivity, is necessary to maximize their therapeutic potential while minimizing drawbacks in peripheral nerve regeneration.

The first step of this study involved coating the pure Mg surface with HA, and then followed by solidification of the GDNF gel on the HA-Mg surface. The dual coating of GDNF-Gel/HA-Mg enhanced the surface properties of pure Mg. Previous study showed that the surface properties of biomaterials such as roughness, wettability, and chemical composition are of great importance in practical application [32]. GDNF-Gel/HA-Mg, with an average roughness of 3.29 μm, allowed cells to grow. Although the contact angle of GDNF-Gel/HA-Mg was significantly lower than that of pure Mg, it still showed good hydrophilicity. The wettability of a biomaterial surface plays a crucial role in the adsorption of adhesion-related proteins, such as fibronectin and laminin, from the culture medium. A moderately hydrophilic surface has been shown to facilitate protein adsorption, thereby enhancing cell adhesion [33]. As illustrated in Fig. 2C, the contact angle on the pure Mg surface was 86.59°, whereas it decreased to 66.05°on the GDNF-Gel/HA-Mg surface. This improvement in hydrophilicity can be attributed to the presence of hydrophilic functional groups in the coating, which may enhance protein adsorption and provide a more favorable environment for cell attachment. Additionally, surface roughness provides essential micro/nanoscale topographical cues that increase the effective contact area, promote adhesion protein deposition, and influence cytoskeletal remodeling, thereby regulating cell adhesion, migration, and proliferation [32,34]. As shown in Fig. 2D, the 3D roughness analysis of the GDNF-Gel/HA-Mg surface revealed the formation of micro-pores and surface irregularities. While the local maximum height difference

reached 131.89 μm, the overall surface roughness remained at 3.29 μm, these structural features may contribute to improved protein adsorption and cellular interactions. Therefore, the optimized wettability and appropriate surface roughness of the GDNF-Gel/HA-Mg coating work synergistically to create a microenvironment conducive to cell adhesion and growth.

GDNF-Gel as the outermost layer, also played a significant role in the corrosion control and biological performance of the internal layer. Utilizing a physical barrier to block the corrosive medium, GDNF-Gel reduced the degradation rate of HA-Mg and its protective effect disappeared after shedding or degradation. The GDNF-Gel/HA-Mg exhibited the lowest corrosion current density, the highest corrosion potential and impedance in PBS solution. Although the electrochemical test is a short-term experiment [35], the results that the GDNF-Gel/HA-Mg enhanced the corrosion resistance of pure Mg were supported by the immersion and hydrogen evolution experiments, the GDNF-Gel/HA-Mg showed a slower pH increase, and lower release of Mg^{2+} and Ca^{2+} ions in PBS solution, owing to the coating that impeded water diffusion and ion assault. Additionally, GDNF-Gel/HA-Mg kept steady, and the slowest release profile with a calculated corrosion rate of 0.13 mm/y on day 28, which represented a considerable enhancement of corrosion resistance by 23.53 % and 50 % compared to HA-Mg and pure Mg, respectively. These results indicate that the corrosion of pure Mg in PBS solution was retarded by the HA coating in conjunction with the GDNF-Gel layer.

In this study, we utilized GelMA hydrogel to load GDNF and prepared GDNF-Gel/HA-Mg. Live/dead staining results demonstrated that GDNF-Gel/HA-Mg exhibited good biocompatibility and did not exhibit significant cytotoxicity on Schwann cells. Schwann cells, as the major non-neuronal active cells in the neural stem, play a vital role in neurotrophic support, chemotaxis, and maturation of regenerating nerve fibers [36]. The results showed that GDNF-Gel/HA-Mg could enhance the proliferation, migration abilities of Schwann cells, as well as promote the dedifferentiation process, thereby facilitating the regeneration and repair of peripheral nerve tissue.

Netrin-1 serves as a critical regulator in neural development, orchestrating Schwann cells proliferation and axonal extension through dynamically upregulated expression following PNI [37]. Mechanistically, Schwann cells exhibit preferential expression of UNC5b over other Netrin-1 receptors (Neogenin/UNC5a), with UNC5b-Netrin-1 binding not only potentiating Schwann cells proliferation but also inducing membrane-localized signaling complexes that activate AMPK/ULK1 phosphorylation cascades - a dual mechanism enhancing Schwann cells autophagy while suppressing apoptosis [37,38]. Our studies reveal that GDNF-Gel/HA-Mg composites recapitulate these neuroregenerative effects, significantly boosting Schwann cells proliferation and oxidative stress resistance via Netrin-1/UNC5b pathway activation. Rac1 and Cdc42, small GTPases from the Ras family, play an indispensable role in Schwann cells' cellular biology [39,40]. Under external signals such as G protein-coupled receptor stimulation, these genes are rapidly activated, leading to remodeling of the cytoskeleton. This remodeling process is essential for regulating various cellular activities in Schwann cells, including proliferation and migration. Activated Rac1 and Cdc42 primarily participate in the formation of lamellipodia and filopodia, thus promoting Schwann cells migration and achieving directional movement [39–41]. Our study suggested that GDNF-Gel/HA-Mg can effectively promote the migration of Schwann cells, and based on the findings showing that GDNF-Gel/HA-Mg enhances the expression levels of Rac1 and Cdc42 proteins, it can be inferred that this mechanism of promoting cell migration is likely mediated through the activation of Rac1 and Cdc42 expression.

Following PNI, the affected area and its distant end suffer from ischemia and inflammation, leading to a notable rise in ROS [42,43]. Excessive ROS disrupts the balance between cellular oxidation and antioxidant processes, triggering oxidative stress reactions that inflict damage on lipids, proteins, and DNA, ultimately resulting in cell apoptosis [44,45]. GDNF-Gel/HA-Mg holds the potential to alleviate oxidative stress induced by PNI, decrease ROS production, protect Schwann cells and neurons against apoptosis, and create a conducive microenvironment for peripheral nerve regeneration. This might be attributed to the release of Mg from GDNF-Gel/HA-Mg. Previous studies have showed that Mg mitigates intracellular ROS generation through several mechanisms, including antioxidant enzyme modulation, cell membrane stability, and metabolic regulation [46–51]: Mg is a crucial cofactor for key antioxidant enzymes like superoxide dismutase (SOD) and glutathione peroxidase (GSH-Px). It stabilizes the structure of Mn-SOD, enhancing its ability to reduce ROS production, additionally, Mg maintains GSH-Px activity, preventing H_2O_2 accumulation and further ROS generation [50,51]. It also suppresses ROS by interacting with NADPH oxidase subunits [49]. Moreover, Mg regulates ion channels, particularly calcium channels, preventing intracellular calcium overload and the activation of ROS-producing pathways. Furthermore, Mg influences mitochondrial function by regulating the TCA cycle and pyruvate dehydrogenase complex activity, minimizing electron leakage in the electron transport chain and reducing ROS generation [48,51]. It also buffers intracellular pH, preventing an acidic environment from activating ROS-producing enzymes [50].

Moreover, by modulating the M2 macrophage polarization process within the microenvironment surrounding the injured nerves, GDNF-Gel/HA-Mg not only suppresses inflammation but also facilitates the regeneration of peripheral nerve. M1 macrophages predominantly mediate the release of pro-inflammatory cytokines, which can prolong the nerve repair process and exacerbate tissue damage [52]. Conversely, M2 macrophages play a crucial role in orchestrating anti-inflammatory responses and promoting angiogenesis, thereby accelerating the repair of PNI. Through the secretion of key anti-inflammatory cytokines such as IL-10 and TGF-β, M2 macrophages effectively attenuate the inflammatory response after PNI, minimizing inflammation-induced damage and fostering a more conducive microenvironment for nerve regeneration [53]. Moreover, M2 macrophages secrete vascular endothelial growth factor (VEGF) and neurotrophic factors, which not only enhance neovascularization but also support neuronal survival and functional recovery [54,55]. Given these mechanisms, GDNF-Gel/HA-Mg serves as a potent modulator of macrophage polarization, fine-tuning the balance between pro-inflammatory and anti-inflammatory mediators. By mitigating excessive inflammation and optimizing the inflammatory milieu, it helps counteract the deleterious effects of prolonged inflammation on nerve regeneration. Ultimately, by establishing a more regenerative microenvironment, GDNF-Gel/HA-Mg significantly enhances the repair and regeneration of peripheral nerve tissues. This effect was confirmed by the *in vivo* research, which showed that GDNF-Gel/HA-Mg could significantly promote the regeneration of sciatic nerve, as well as myelination of regenerated nerves, leading to the prevention of denervated gastrocnemius atrophy.

Our study has certain limitations. The precise molecular mechanisms underlying the immunomodulatory effects of GDNF-Gel/HA-Mg, particularly its role in regulating macrophage polarization and neurotrophic factor release, remain to be fully elucidated. Future research should focus on further clarifying these mechanisms through advanced molecular and transcriptomic analyses. Additionally, while our *in vivo* model demonstrates promising functional recovery, long-term evaluations and large-animal studies are necessary to confirm its clinical feasibility and safety.

From a translational perspective, the successful application of GDNF-Gel/HA-Mg in clinical settings may face challenges related to manufacturing scalability, long-term biocompatibility, and degradation kinetics under physiological conditions. Future studies should explore optimized fabrication techniques and customized degradation profiles to align with the dynamic process of nerve regeneration. Despite these challenges, the dual-modification strategy employed in this study provides a foundation for further development of bioactive magnesium-based nerve conduits, with the ultimate goal of translating these

materials into clinical practice for improved nerve repair outcomes.

6. Conclusion

1) GDNF-Gel/HA-Mg exhibits good hydrophilicity and suitable roughness, which can promote cell adhesion. Meanwhile, GDNF-Gel/HA-Mg enhances the corrosion resistance of pure Mg in PBS solution, providing sufficient mechanical support and axial guidance during nerve regeneration.
2) GDNF-Gel/HA-Mg could promote Schwann cell proliferation, migration, invasion, and secretion of NGF. Additionally, it could induce Schwann cell dedifferentiation, thereby facilitating peripheral nerve regeneration.
3) GDNF-Gel/HA-Mg could facilitate the process of nerve regeneration and myelination, which might be provided as an ideal candidate for peripheral nerve defects repairment.

CRediT authorship contribution statement

Yuanqing Cai: Writing – original draft, Investigation. **Yi Chen:** Writing – original draft, Investigation. **Hongyan Li:** Visualization, Methodology, Data curation. **Yanyu Wang:** Visualization, Methodology, Data curation. **Guangyang Zhang:** Visualization, Methodology, Data curation. **Jialin Liang:** Visualization, Methodology, Data curation. **Leifeng Lv:** Formal analysis. **Ying Huang:** Formal analysis. **Wenming Zhang:** Formal analysis. **Xiaoqian Dang:** Conceptualization. **Xinyu Fang:** Conceptualization. **Yong Wang:** Conceptualization.

Ethics approval and consent to participate

Not applicable.

Funding

This work was supported by National Natural Science Foundation of China (82171370); Joint Funds for the Innovation of Science and Technology, Fujian Province (2021Y9125; 2024Y9159). These funders were not involved in any aspects regarding conduction, analysis, interpretation, or publication of the study.

Declaration of competing interest

The authors declare that they have no known competing financial interests or personal relationships that could have appeared to influence the work reported in this paper.

Acknowledgments

Not applicable.

Appendix A. Supplementary data

Supplementary data to this article can be found online at https://doi.org/10.1016/j.mtbio.2025.101764.

Data availability

Data will be made available on request.

References

[1] G. Li, Q. Han, P. Lu, L. Zhang, Y. Zhang, S. Chen, et al., Construction of dual-biofunctionalized chitosan/collagen scaffolds for simultaneous neovascularization and nerve regeneration, Res (Washington, DC) 2020 (2020) 2603048, https://doi.org/10.34133/2020/2603048.
[2] H. Yildiran, M.S. Macit, G. Özata Uyar, New approach to peripheral nerve injury: nutritional therapy, Nutr. Neurosci. 23 (2020) 744–755, https://doi.org/10.1080/1028415X.2018.1554322.
[3] X. Yang, R. Liu, Y. Xu, X. Ma, B. Zhou, The mechanisms of peripheral nerve preconditioning injury on promoting axonal regeneration, Neural Plast. 2021 (2021) 6648004, https://doi.org/10.1155/2021/6648004.
[4] B. Battiston, P. Titolo, D. Ciclamini, B. Panero, Peripheral nerve defects: overviews of practice in europe, Hand Clin. 33 (2017) 545–550, https://doi.org/10.1016/j.hcl.2017.04.005.
[5] T. Kornfeld, P.M. Vogt, C. Radtke, Nerve grafting for peripheral nerve injuries with extended defect sizes, Wien. Med. Wochenschr. 169 (2019) 240–251, https://doi.org/10.1007/s10354-018-0675-6.
[6] L.B. Dahlin, Techniques of peripheral nerve repair, Scand. J. Surg. 97 (2008) 310–316, https://doi.org/10.1177/145749690809700407.
[7] A. Pabari, H. Lloyd-Hughes, A.M. Seifalian, A. Mosahebi, Nerve conduits for peripheral nerve surgery, Plast. Reconstr. Surg. 133 (2014) 1420–1430, https://doi.org/10.1097/PRS.0000000000000226.
[8] Q. Lu, F. Zhang, W. Cheng, X. Gao, Z. Ding, X. Zhang, et al., Nerve guidance conduits with hierarchical anisotropic architecture for peripheral nerve regeneration, Adv Healthc Mater 10 (2021) e2100427, https://doi.org/10.1002/adhm.202100427.
[9] S. Song, X. Wang, T. Wang, Q. Yu, Z. Hou, Z. Zhu, et al., Additive manufacturing of nerve guidance conduits for regeneration of injured peripheral nerves, Front. Bioeng. Biotechnol. 8 (2020) 590596, https://doi.org/10.3389/fbioe.2020.590596.
[10] R.G. Sabongi, M. Fernandes, J.B.G. Dos Santos, Peripheral nerve regeneration with conduits: use of vein tubes, Neural Regen Res 10 (2015) 529–533, https://doi.org/10.4103/1673-5374.155428.
[11] S. Geuna, P. Tos, B. Battiston, M.G. Giacobini-Robecchi, Bridging peripheral nerve defects with muscle-vein combined guides, Neurol. Res. 26 (2004) 139–144, https://doi.org/10.1179/016164104225013752.
[12] P. Konofaos, J.P. Ver Halen, Nerve repair by means of tubulization: past, present, future, J. Reconstr. Microsurg. 29 (2013) 149–164, https://doi.org/10.1055/s-0032-1333316.
[13] Q. Long, B. Wu, Y. Yang, S. Wang, Y. Shen, Q. Bao, et al., Nerve guidance conduit promoted peripheral nerve regeneration in rats, Artif. Organs 45 (2021) 616–624, https://doi.org/10.1111/aor.13881.
[14] W. Chang, M.B. Shah, P. Lee, X. Yu, Tissue-engineered spiral nerve guidance conduit for peripheral nerve regeneration, Acta Biomater. 73 (2018) 302–311, https://doi.org/10.1016/j.actbio.2018.04.046.
[15] P. Zhang, F. Xue, Y. Kou, Z. Fu, D. Zhang, H. Zhang, et al., The experimental study of absorbable chitin conduit for bridging peripheral nerve defect with nerve fasciculu in rats, Artif. Cells Blood Substit. Immobil. Biotechnol. 36 (2008) 360–371, https://doi.org/10.1080/10731190802239040.
[16] N. Wang, S. Yang, H. Shi, Y. Song, H. Sun, Q. Wang, et al., Magnesium alloys for orthopedic applications:A review on the mechanisms driving bone healing, J. Magnesium Alloys 10 (2022) 3327–3353, https://doi.org/10.1016/j.jma.2022.11.014.
[17] A.M.P. Romani, Cellular magnesium homeostasis, Arch. Biochem. Biophys. 512 (2011) 1–23, https://doi.org/10.1016/j.abb.2011.05.010.
[18] J.H.F. de Baaij, J.G.J. Hoenderop, R.J.M. Bindels, Magnesium in man: implications for health and disease, Physiol. Rev. 95 (2015) 1–46, https://doi.org/10.1152/physrev.00012.2014.
[19] J. Zhang, B. Zhang, J. Zhang, W. Lin, S. Zhang, Magnesium promotes the regeneration of the peripheral nerve, Front. Cell Dev. Biol. 9 (2021) 717854, https://doi.org/10.3389/fcell.2021.717854.
[20] Z. Yao, W. Yuan, J. Xu, W. Tong, J. Mi, P.-C. Ho, et al., Magnesium-Encapsulated injectable hydrogel and 3D-engineered polycaprolactone conduit facilitate peripheral nerve regeneration, Adv Sci (Weinheim, Baden-Wurttemberg, Ger 9 (2022) e2202102, https://doi.org/10.1002/advs.202202102.
[21] H.-C. Pan, M.-L. Sheu, H.-L. Su, Y.-J. Chen, C.-J. Chen, D.-Y. Yang, et al., Magnesium supplement promotes sciatic nerve regeneration and down-regulates inflammatory response, Magnes. Res. 24 (2011) 54–70, https://doi.org/10.1684/mrh.2011.0280.
[22] B.-H. Li, K. Yang, X. Wang, Biodegradable magnesium wire promotes regeneration of compressed sciatic nerves, Neural Regen Res 11 (2016) 2012–2017, https://doi.org/10.4103/1673-5374.197146.
[23] X. Li, R. Filek, X. Zhu, H. Gao, L. Qiao, H. Liu, et al., Bio-modulation of scaring Glaucoma Filtration Surgery using a novel application of coated magnesium, J. Magnesium Alloys 9 (2021) 883–894, https://doi.org/10.1016/j.jma.2020.02.025.
[24] Z. Shi, M. Liu, A. Atrens, Measurement of the corrosion rate of magnesium alloys using Tafel extrapolation, Corros. Sci. 52 (2010) 579–588, https://doi.org/10.1016/j.corsci.2009.10.016.
[25] G. Song, A. Atrens, D. Suohn, An hydrogen evolution method for the estimation of the corrosion rate of magnesium alloys, in: Essent. Readings Magnes. Technol., John Wiley & Sons, Inc., Hoboken, NJ, USA, 2014, pp. 565–572, https://doi.org/10.1002/9781118859803.ch90.
[26] M.P. Moreira, G.D. de Almeida Soares, J. Dentzer, K. Anselme, L.Á. de Sena, A. Kuznetsov, et al., Synthesis of magnesium- and manganese-doped hydroxyapatite structures assisted by the simultaneous incorporation of strontium, Mater. Sci. Eng. C 61 (2016) 736–743, https://doi.org/10.1016/j.msec.2016.01.004.
[27] D. Mu, J. Xing, The preparation of double network hydrogel with high mechanical properties by photopolymerization under the green LED irradiation and

enhancement of wet adhesion by tannic acid, Colloids Surfaces A Physicochem Eng Asp 671 (2023) 131656, https://doi.org/10.1016/j.colsurfa.2023.131656.
[28] H. Zhang, R. Luo, W. Li, J. Wang, M.F. Maitz, J. Wang, et al., Epigallocatechin gallate (EGCG) induced chemical conversion coatings for corrosion protection of biomedical MgZnMn alloys, Corros. Sci. 94 (2015) 305–315, https://doi.org/10.1016/j.corsci.2015.02.015.
[29] Z. Jia, P. Xiong, Y. Shi, W. Zhou, Y. Cheng, Y. Zheng, et al., Inhibitor encapsulated, self-healable and cytocompatible chitosan multilayer coating on biodegradable Mg alloy: a pH-responsive design, J. Mater. Chem. B 4 (2016) 2498–2511, https://doi.org/10.1039/C6TB00117C.
[30] T.M. Hopkins, K.J. Little, J.J. Vennemeyer, J.L. Triozzi, M.K. Turgeon, A. M. Heilman, et al., Short and long gap peripheral nerve repair with magnesium metal filaments, J. Biomed. Mater. Res. 105 (2017) 3148–3158, https://doi.org/10.1002/jbm.a.36176.
[31] A.A. Almansoori, K.W. Ju, B. Kim, S.M. Kim, S.-M. Lee, J.-H. Lee, Hydroxyapatite coated magnesium alloy for peripheral nerve regeneration, Oral Biol Res 42 (2018) 105–113, https://doi.org/10.21851/obr.42.03.201809.105.
[32] T.T. Paterlini, L.F.B. Nogueira, C.B. Tovani, M.A.E. Cruz, R. Derradi, A.P. Ramos, The role played by modified bioinspired surfaces in interfacial properties of biomaterials, Biophys Rev 9 (2017) 683–698, https://doi.org/10.1007/s12551-017-0306-2.
[33] S.A. Redey, M. Nardin, D. Bernache-Assolant, C. Rey, P. Delannoy, L. Sedel, et al., Behavior of human osteoblastic cells on stoichiometric hydroxyapatite and type A carbonate apatite: role of surface energy, J. Biomed. Mater. Res. 50 (2000) 353–364, https://doi.org/10.1002/(SICI)1097-4636(20000605)50:3<353::AID-JBM9>3.0.CO;2-C.
[34] S. Spriano, M. Bosetti, M. Bronzoni, E. Vernè, G. Maina, V. Bergo, et al., Surface properties and cell response of low metal ion release Ti-6Al-7Nb alloy after multi-step chemical and thermal treatments, Biomaterials 26 (2005) 1219–1229, https://doi.org/10.1016/j.biomaterials.2004.04.026.
[35] Y. Chen, J. Yan, Z. Wang, S. Yu, X. Wang, Z. Yuan, et al., In vitro and in vivo corrosion measurements of Mg–6Zn alloys in the bile, Mater. Sci. Eng. C 42 (2014) 116–123, https://doi.org/10.1016/j.msec.2014.05.014.
[36] K.R. Jessen, R. Mirsky, A.C. Lloyd, Schwann cells: development and role in nerve repair, Cold Spring Harbor Perspect. Biol. 7 (2015) a020487, https://doi.org/10.1101/cshperspect.a020487.
[37] X.-P. Dun, D.B. Parkinson, Role of netrin-1 signaling in nerve regeneration, Int. J. Mol. Sci. 18 (2017), https://doi.org/10.3390/ijms18030491.
[38] H.K. Lee, I.A. Seo, E. Seo, S.-Y. Seo, H.J. Lee, H.T. Park, Netrin-1 induces proliferation of Schwann cells through Unc5b receptor, Biochem. Biophys. Res. Commun. 362 (2007) 1057–1062, https://doi.org/10.1016/j.bbrc.2007.08.143.
[39] J. Yamauchi, Y. Miyamoto, A. Tanoue, E.M. Shooter, J.R. Chan, Ras activation of a Rac1 exchange factor, Tiam1, mediates neurotrophin-3-induced Schwann cell migration, Proc. Natl. Acad. Sci. U. S. A. 102 (2005) 14889–14894, https://doi.org/10.1073/pnas.0507125102.
[40] B. Han, J.-Y. Zhao, W.-T. Wang, Z.-W. Li, A.-P. He, X.-Y. Song, Cdc42 promotes Schwann cell proliferation and migration through wnt/β-catenin and p38 MAPK signaling pathway after sciatic nerve injury, Neurochem. Res. 42 (2017) 1317–1324, https://doi.org/10.1007/s11064-017-2175-2.
[41] E. Mantuano, M. Jo, S.L. Gonias, W.M. Campana, Low density lipoprotein receptor-related protein (LRP1) regulates Rac1 and RhoA reciprocally to control Schwann cell adhesion and migration, J. Biol. Chem. 285 (2010) 14259–14266, https://doi.org/10.1074/jbc.M109.085126.
[42] I. Ullah, Y.-H. Choe, M. Khan, D. Bharti, S.B. Shivakumar, H.-J. Lee, et al., Dental pulp-derived stem cells can counterbalance peripheral nerve injury-induced oxidative stress and supraspinal neuro-inflammation in rat brain, Sci. Rep. 8 (2018) 15795, https://doi.org/10.1038/s41598-018-34151-x.
[43] H. Wang, X.-G. Ding, S.-W. Li, H. Zheng, X.-M. Zheng, S. Navin, et al., Role of oxidative stress in surgical cavernous nerve injury in a rat model, J. Neurosci. Res. 93 (2015) 922–929, https://doi.org/10.1002/jnr.23545.
[44] Y. Qian, Q. Han, X. Zhao, J. Song, Y. Cheng, Z. Fang, et al., 3D melatonin nerve scaffold reduces oxidative stress and inflammation and increases autophagy in peripheral nerve regeneration, J. Pineal Res. 65 (2018) e12516, https://doi.org/10.1111/jpi.12516.
[45] G. Cheng, X. Liu, Y. Liu, Y. Liu, R. Ma, J. Luo, et al., Ultrasmall coordination polymers for alleviating ROS-mediated inflammatory and realizing neuroprotection against Parkinson's disease, Res (Washington, DC) 2022 (2022) 9781323, https://doi.org/10.34133/2022/9781323.
[46] C. Cao, P. Yu, C. Chu, Z. Wang, W. Xu, F. Cheng, et al., Magnesium hydride attenuates intestinal barrier injury during hemorrhage shock by regulating neutrophil extracellular trap formation via the ROS/MAPK/PAD4 pathway, Int. Immunopharmacol. 130 (2024) 111688, https://doi.org/10.1016/j.intimp.2024.111688.
[47] F. Hoşgörler, S. Kızıldağ, M. Ateş, A. Argon, B. Koç, S. Kandis, et al., The chronic use of magnesium decreases VEGF levels in the uterine tissue in rats, Biol. Trace Elem. Res. 196 (2020) 545–551, https://doi.org/10.1007/s12011-019-01944-8.
[48] H. Zhou, Z. He, Y. Cao, L. Chu, B. Liang, K. Yu, et al., An injectable magnesium-loaded hydrogel releases hydrogen to promote osteoporotic bone repair via ROS scavenging and immunomodulation, Theranostics 14 (2024) 3739–3759, https://doi.org/10.7150/thno.97412.
[49] J.B.S. Morais, J.S. Severo, LR Dos Santos, S.R. de Sousa Melo, R. de Oliveira Santos, A.R.S. de Oliveira, et al., Role of magnesium in oxidative stress in individuals with obesity, Biol. Trace Elem. Res. 176 (2017) 20–26, https://doi.org/10.1007/s12011-016-0793-1.
[50] R.D. Bukoski, Reactive oxygen species: the missing link between magnesium deficiency and hypertension? J. Hypertens. 20 (2002) 2141–2143, https://doi.org/10.1097/00004872-200211000-00009.
[51] R. Scrimieri, L. Locatelli, R. Cazzola, J.A.M. Maier, A. Cazzaniga, Reactive oxygen species are implicated in altering magnesium homeostasis in endothelial cells exposed to high glucose, Magnes. Res. 32 (2019) 54–62, https://doi.org/10.1684/mrh.2019.0456.
[52] X. Li, X. Li, J. Yang, Y. Du, L. Chen, G. Zhao, et al., In situ sustained macrophage-targeted nanomicelle-hydrogel microspheres for inhibiting osteoarthritis, Res (Washington, DC) 6 (2023) 131, https://doi.org/10.34133/research.0131.
[53] P. Liu, J. Peng, G.-H. Han, X. Ding, S. Wei, G. Gao, et al., Role of macrophages in peripheral nerve injury and repair, Neural Regen Res 14 (2019) 1335–1342, https://doi.org/10.4103/1673-5374.253510.
[54] A.-L. Cattin, J.J. Burden, L. Van Emmenis, F.E. Mackenzie, J.J.A. Hoving, N. Garcia Calavia, et al., Macrophage-induced blood vessels guide Schwann cell-mediated regeneration of peripheral nerves, Cell 162 (2015) 1127–1139, https://doi.org/10.1016/j.cell.2015.07.021.
[55] Y. Li, S. Kang, D. Halawani, Y. Wang, C. Junqueira Alves, A. Ramakrishnan, et al., Macrophages facilitate peripheral nerve regeneration by organizing regeneration tracks through Plexin-B2, Genes Dev. 36 (2022) 133–148, https://doi.org/10.1101/gad.349063.121.